

1 **Reviewing Global Estimates of Surface Reactive Nitrogen Concentration and**  
2 **Deposition Using Satellite Retrievals**

3 Lei Liu <sup>a,\*</sup>, Xiuying Zhang <sup>b</sup>, Wen Xu <sup>c</sup>, Xuejun Liu <sup>c</sup>, Xuehe Lu <sup>b</sup>, Jing Wei <sup>d,e</sup>, Yi Li <sup>f</sup>,  
4 Yuyu Yang <sup>a</sup>, Zhen Wang <sup>b</sup>, Anthony Y. H. Wong <sup>g</sup>

5 <sup>a</sup> College of Earth and Environmental Sciences, Lanzhou University, Lanzhou 730000,  
6 China

7 <sup>b</sup> International Institute for Earth System Science, Nanjing University, Nanjing,  
8 210023, China

9 <sup>c</sup> College of Resources and Environmental Sciences, National Academy of  
10 Agriculture Green Development, China Agricultural University, Beijing, 100193,  
11 China

12 <sup>d</sup> State Key Laboratory of Remote Sensing Science, College of Global Change and  
13 Earth System Science, Beijing Normal University, Beijing, China

14 <sup>e</sup> Department of Atmospheric and Oceanic Science, Earth System Science  
15 Interdisciplinary Center, University of Maryland, College Park, MD, USA

16 <sup>f</sup> Chief Technology Officer SailBri Cooper Inc., Beaverton OR, 97008, USA

17 <sup>g</sup> Department of Earth and Environment, Boston University, Boston, MA 02215, USA

18 \* Correspondence to Lei Liu (liuleigeo@lzu.edu.cn).

19 **Abstract**

20 Since the industrial revolution, human activities have dramatically changed the  
21 nitrogen (N) cycle in natural systems. Anthropogenic emissions of reactive nitrogen  
22 ( $N_r$ ) can return to the earth's surface through atmospheric  $N_r$  deposition. Increased  $N_r$   
23 deposition may improve ecosystem productivity. However, excessive  $N_r$  deposition  
24 can cause a series of negative effects on ecosystem health, biodiversity, soil, and  
25 water. Thus, accurate estimations of  $N_r$  deposition are necessary for evaluating its

26 environmental impacts. The United States, Canada and Europe have successively  
27 launched a number of satellites with sensors that allow retrieval of atmospheric NO<sub>2</sub>  
28 and NH<sub>3</sub> column density, and therefore estimation of surface N<sub>r</sub> concentration and  
29 deposition at an unprecedented spatiotemporal scale. Atmosphere NH<sub>3</sub> column can be  
30 retrieved from atmospheric infra-red emission, while atmospheric NO<sub>2</sub> column can be  
31 retrieved from reflected solar radiation. In recent years, scientists attempted to  
32 estimate surface N<sub>r</sub> concentration and deposition using satellite retrieval of  
33 atmospheric NO<sub>2</sub> and NH<sub>3</sub> columns. In this study, we give a thorough review on  
34 recent advances of estimating surface N<sub>r</sub> concentration and deposition using the  
35 satellite retrievals of NO<sub>2</sub> and NH<sub>3</sub>, present a framework of using satellite data to  
36 estimate surface N<sub>r</sub> concentration and deposition based on recent works, and  
37 summarize the existing challenges for estimating surface N<sub>r</sub> concentration and  
38 deposition using the satellite-based methods. We believe that exploiting satellite data  
39 to estimate N<sub>r</sub> deposition has a broad and promising prospect.

#### 40 **Keywords**

41 Nitrogen deposition; Satellite retrieval; Surface concentration; Oxidized and reduced  
42 N<sub>r</sub>

#### 43 **1. Introduction**

44 Nitrogen (N) exists in three forms in the environment including reactive nitrogen (N<sub>r</sub>),  
45 organic nitrogen (ON) and nitrogen gas (N<sub>2</sub>) (Canfield et al., 2010). N<sub>2</sub> is the main  
46 component of air, accounting for 78% of the total volume of air, but it cannot be  
47 directly used by most plants. N<sub>r</sub> refers to the general term of N-containing substances  
48 in atmosphere, plants, soils and fertilizers that are not combined with carbon. N<sub>r</sub> (such  
49 as NO<sub>3</sub><sup>-</sup> and NH<sub>4</sub><sup>+</sup>) is the main form of N that can be directly used by most plants, but  
50 the content of N<sub>r</sub> in nature is much lower compared with ON and N<sub>2</sub> (Vitousek et al.,

51 1997;Nicolas and Galloway, 2008). The supply of  $N_r$  is essential for all life forms and  
52 contributes to the increase in agricultural production, thus providing sufficient food  
53 for the growing global population (Galloway et al., 2008;David et al., 2013;Galloway  
54 et al., 2004b;Erisman et al., 2008). Before the industrial revolution,  $N_r$  mainly came  
55 from natural sources such as biological N fixation, lightning and volcanic eruption  
56 (Galloway et al., 2004a). Since the industrial revolution, human activities (e.g.  
57 agricultural development, combustion of fossil energy) have greatly perturbed the N  
58 cycle in natural systems (Canfield et al., 2010;Kim et al., 2014;Lamarque et al.,  
59 2005).

60  $N_r$  ( $NO_x$  and  $NH_3$ ) emitted to the atmosphere will return to the earth surface through  
61 atmospheric deposition (Liu et al., 2011). Atmospheric  $N_r$  deposition refers to the  
62 process in which  $N_r$  are removed from the atmosphere, including wet (rain and snow)  
63 and dry (gravitational settling, atmospheric turbulence, etc.) deposition (Xu et al.,  
64 2015;Zhang et al., 2012;Pan et al., 2012). The input of  $N_r$  over terrestrial natural  
65 ecosystems primarily comes from the  $N_r$  deposition (Shen et al., 2013;Sutton et al.,  
66 2001;Larssen et al., 2011). In the short term, atmospheric  $N_r$  deposition can increase  
67 the  $N_r$  input to ecosystems, which promotes plant growth and enhances ecosystem  
68 productivity (Erisman et al., 2008;Sutton et al., 2013). However, excessive  
69 atmospheric  $N_r$  deposition also causes a series of environmental problems (Liu et al.,  
70 2017d). Due to the low efficiency of agricultural N application, plenty of  $N_r$  is lost  
71 through runoff, leaching and volatilization, causing serious environmental pollution.  
72 Excessive  $N_r$  deposition may aggravate the plant's susceptibility to drought or frost,  
73 reduce the resistance of plant to pathogens or pests, and further affect the physiology  
74 and biomass distribution of vegetation (ratio of roots, stems and leaves) (Stevens et al.,  
75 2004;Nadelhoffer et al., 1999;Bobbink et al., 2010;Janssens et al., 2010). Excessive

76  $N_r$  leads to eutrophication and related algal blooms over aquatic ecosystems, reducing  
77 water biodiversity (Paerl et al., 2014), while excessive  $N_r$  in drinking water also poses  
78 a threat to human health (Zhao et al., 2013; Wei et al., 2019). Therefore, monitoring  
79 and estimation of surface  $N_r$  concentration and deposition on the global scale are of  
80 great importance and urgency.

81 The methods of estimating atmospheric  $N_r$  deposition can be divided into three  
82 categories: ground-based monitoring, atmospheric chemical transport modeling  
83 (ACTM) and satellite-based estimation. Ground-based monitoring is considered to be  
84 the most accurate and quantitative method, which can effectively reflect the  $N_r$   
85 deposition in local areas. ACTM can simulate the processes of  $N_r$  chemical reaction,  
86 transport, and deposition, as well as the vertical distribution of  $N_r$ . Satellite-based  
87 estimation establishes empirical, physical or semi-empirical models by connecting the  
88 ground-based  $N_r$  concentrations and deposition with satellite-derived  $N_r$  concentration.  
89 This study focuses on reviewing the recent development of satellite-based methods to  
90 estimate  $N_r$  deposition. Since the estimation of  $N_r$  concentrations is just a part of the  
91 estimation of dry  $N_r$  depositions, we here mainly reviewed the progress of dry  $N_r$   
92 depositions using the satellite observation. We firstly give a brief introduction to the  
93 progress of ground-based monitoring, ACTM-based methods, and then present a  
94 detailed framework of using satellite observation to estimate dry and wet  $N_r$   
95 deposition (including both oxidized and reduced  $N_r$ ). Next, we review the recent  
96 advances of the satellite-based methods of estimating  $N_r$  deposition. Finally, we  
97 discuss the remaining challenges for estimating surface  $N_r$  concentration and  
98 deposition using satellite observation.

## 99 **2 Methods for Estimating Surface $N_r$ Concentration and Deposition**

### 100 **2.1 Ground-based Monitoring**

101 Ground-based monitoring of  $N_r$  deposition can be divided into two parts: wet and dry  
102  $N_r$  deposition monitoring. Since the 1970s, there have been large-scale monitoring  
103 networks focusing on the wet  $N_r$  deposition. The main large-scale regional monitoring  
104 networks include Canadian Air and Precipitation Monitoring Network (CAPMoN),  
105 Acid Deposition Monitoring Network in East Asia (EANET), European Monitoring  
106 and Evaluation Program (EMEP), United States National Atmospheric Deposition  
107 Program (NADP), World Meteorological Organization Global Atmosphere Watch  
108 Precipitation Chemistry Program, and Nationwide Nitrogen Deposition Monitoring  
109 Network in China (NNDMN) (Tan et al., 2018; Vet et al., 2014). The detailed  
110 scientific objectives of the wet  $N_r$  deposition observation networks vary, but most of  
111 the observation networks mainly concentrate on the spatiotemporal variation of wet  
112 deposition of ions including  $N_r$  compounds, the long-term trends of ions in  
113 precipitation, and the evaluation of ACTMs.

114 Compared with wet  $N_r$  deposition monitoring, dry  $N_r$  deposition monitoring started  
115 late, due to the limitation of monitoring technology since it is more difficult to be  
116 quantified (affected greatly by surface roughness, air humidity, climate and other  
117 environmental factors) (Liu et al., 2017c). Dry  $N_r$  deposition observation networks  
118 include US ammonia monitoring network (AMoN), CAPMoN, EANET and EMEP.  
119 The monitoring methods of dry  $N_r$  deposition are mainly divided into direct  
120 monitoring (such as dynamic chambers) and indirect monitoring (such as inferential  
121 methods). The inferential model is widely applied in ground-based monitoring  
122 networks (such as EANET and NNDMN), mainly because this method is more  
123 practical and simpler. In inferential models, dry deposition is divided into two parts:

124 surface  $N_r$  concentrations and the deposition velocity ( $V_d$ ) of  $N_r$  (Nowlan et al., 2014).  
125  $V_d$  can be estimated by meteorology, land use types of underlying surface as well as  
126 the characteristics of each  $N_r$  component itself using resistance models (Nemitz et al.,  
127 2001). Thus, dry  $N_r$  deposition monitoring networks only need to focus on the  
128 quantification of surface concentration of individual  $N_r$  components. The  $N_r$   
129 components in the atmosphere are very complex, including  $N_2O_5$ , HONO,  $NH_3$ ,  $NO_2$ ,  
130  $HNO_3$  and particulate  $NH_4^+$  and  $NO_3^-$ . Most monitoring networks include the major  
131  $N_r$  species such as gaseous  $NH_3$ ,  $NO_2$ ,  $HNO_3$  and the particles of  $NH_4^+$  and  $NO_3^-$ .  
132 Effort of ground-based  $N_r$  deposition monitoring mostly concentrates on wet  $N_r$   
133 deposition, while observations of dry  $N_r$  deposition are relatively scarce especially for  
134 surface  $HNO_3$  and  $NH_4^+$  and  $NO_3^-$ . Second, most observation networks focus on a few  
135 years or a certain period of time, leading to the lack of long-term continuously  
136 monitoring on both wet and dry  $N_r$  deposition. More importantly, the global  $N_r$   
137 deposition monitoring network has not been established, and the sampling standards  
138 in different regions are not unified. These outline the potential room for improvement  
139 of ground-based  $N_r$  deposition monitoring.

## 140 **2.2 Atmospheric Chemistry Transport Model (ACTM) Simulation**

141 An ACTM can simulate  $N_r$  deposition at regional or global scales through explicitly  
142 representing the physical and chemical processes of atmospheric  $N_r$  components  
143 (Zhao et al., 2017; Zhang et al., 2012). Wet  $N_r$  deposition flux is parameterized as  
144 in-cloud, under-cloud and precipitation scavenging (Amos et al., 2012; Levine and  
145 Schwartz, 1982; Liu et al., 2001; Mari et al., 2000), while dry deposition flux can be  
146 obtained as the product of surface  $N_r$  concentration and  $V_d$ , which is typically  
147 parameterized as a network of resistances (Wesely and Hicks, 1977). Based on the  
148 integrated results of 11 models of HTAP (hemispheric transport of air pollution), Tan

149 et al. found that about 76%-83% of the ACTM's simulation results were  $\pm 50\%$  of the  
150 monitoring values, and the modeling results underestimated the wet deposition of  
151  $\text{NH}_4^+$  and  $\text{NO}_3^-$  over Europe and East Asia, and overestimated the wet deposition of  
152  $\text{NO}_3^-$  over the eastern US (Tan et al., 2018). Though regional ACTMs can be  
153 configured at very high horizontal resolution (e.g.,  $1 \times 1 \text{ km}^2$ ) (Kuik et al., 2016), the  
154 horizontal resolution of global ACTMs are relatively coarse ( $1^\circ \times 1^\circ$  to  $5^\circ \times 4^\circ$ ) (Williams  
155 et al., 2017), which cannot indicate the local pattern of  $\text{N}_r$  deposition. On the other  
156 hand, the  $\text{N}_r$  emission inventory used to drive an ACTM is highly uncertain, with the  
157 uncertainty of the  $\text{NO}_x$  emission at about  $\pm 30\text{-}40\%$ , and that of  $\text{NH}_3$  emission at about  
158  $\pm 30\text{-}80\%$  (Zhang et al., 2009; Cao et al., 2011).

### 159 **2.3 Satellite-based Estimation of Surface $\text{N}_r$ Concentration and Deposition**

160 Satellite observation has wide spatial coverages and high resolution, and is  
161 spatiotemporally continuous. Atmospheric  $\text{NO}_2$  and  $\text{NH}_3$  columns can be derived  
162 from satellite measurements with relatively high accuracy (Van Damme et al.,  
163 2014a; Boersma et al., 2011), providing a new perspective about atmospheric  $\text{N}_r$   
164 abundance.

165 Satellite instruments that can monitor  $\text{NO}_2$  in the atmosphere include GOME (Global  
166 Ozone Monitoring Experience), SCIAMACHY (SCanning Imaging Absorption  
167 SpectroMeter for Atmospheric ChartographY), OMI (Ozone Monitoring Instrument),  
168 GOME-2 (Global Ozone Monitoring Experience-2). Some scholars applied satellite  
169  $\text{NO}_2$  columns to estimate the surface  $\text{NO}_2$  concentration, and then dry  $\text{NO}_2$  deposition  
170 by combining the surface  $\text{NO}_2$  concentration and modeled  $V_d$ . Cheng et al. established  
171 a statistical model to estimate the surface  $\text{NO}_2$  concentration based on the  
172 SCIAMACHY  $\text{NO}_2$  columns, and then estimated the dry deposition of  $\text{NO}_2$  over  
173 eastern China (Cheng et al., 2013). This method used the simple linear model and did

174 not consider the vertical profiles of NO<sub>2</sub> (Cheng et al., 2013). Lu et al. established a  
175 multivariate linear regression model based on the SCIAMACHY and GOME NO<sub>2</sub>  
176 columns, meteorological data and ground-based monitoring N<sub>r</sub> deposition, and then  
177 estimated the global total N<sub>r</sub> deposition (Lu et al., 2013). Lu et al. could not  
178 distinguish the contribution of dry and wet N<sub>r</sub> deposition using the multivariate linear  
179 regression model (Lu et al., 2013). Jia et al. established a simple linear regression  
180 model based on OMI tropospheric NO<sub>2</sub> column and ground-based surface N<sub>r</sub>  
181 concentration, and then estimated the total amounts of dry N<sub>r</sub> deposition (Jia et al.,  
182 2016). Jia et al. used OMI tropospheric NO<sub>2</sub> column to estimate the dry deposition of  
183 reduced N<sub>r</sub> deposition (NH<sub>3</sub> and NH<sub>4</sub><sup>+</sup>), which could also bring great errors since the  
184 OMI NO<sub>2</sub> column could not indicate the NH<sub>3</sub> emission. These studies highlight the  
185 problem of using only NO<sub>2</sub> columns to derive total N<sub>r</sub> deposition, that NO<sub>2</sub> columns  
186 give us highly limited information about the abundance of reduced N<sub>r</sub> (NH<sub>3</sub> and  
187 NH<sub>4</sub><sup>+</sup>).

188 Lamsal et al. first used the relationship between the NO<sub>2</sub> column and surface NO<sub>2</sub>  
189 concentration at the bottom layer simulated by an ACTM to convert OMI NO<sub>2</sub>  
190 column to surface NO<sub>2</sub> concentration (Lamsal et al., 2008). A series of works (Lamsal  
191 et al., 2013; Nowlan et al., 2014; Kharol et al., 2018) have effectively estimated  
192 regional and global surface NO<sub>2</sub> concentration using satellite NO<sub>2</sub> column combining  
193 with ACTM-derived relationship between the NO<sub>2</sub> column and surface NO<sub>2</sub>  
194 concentration simulated. It is worth mentioning that Nowlan et al. applied OMI NO<sub>2</sub>  
195 column to obtain the global dry NO<sub>2</sub> deposition during 2005-2007 for the first time  
196 (Nowlan et al., 2014). However, using satellite NO<sub>2</sub> column and ACTM-derived  
197 relationship between the NO<sub>2</sub> column and surface NO<sub>2</sub> concentration may lead to an  
198 underestimation of surface NO<sub>2</sub> concentration. Kharol et al. found that the



199 satellite-derived surface NO<sub>2</sub> concentration using the above method is only half of the  
200 observed values (Kharol et al., 2015). To resolve such potential underestimation,  
201 Larkin et al. established a statistical relationship between the satellite-derived and  
202 ground measured surface NO<sub>2</sub> concentration, and then calibrated the satellite-derived  
203 surface NO<sub>2</sub> concentration using the established relationship (Larkin et al., 2017).

204 Some researchers also estimated other N<sub>r</sub> components (such as particulate NO<sub>3</sub><sup>-</sup>)  
205 based on satellite NO<sub>2</sub> column. Based on the linear model between NO<sub>2</sub>, NO<sub>3</sub><sup>-</sup>, HNO<sub>3</sub>  
206 obtained by ground-based measurements, Jia et al. calculated the surface NO<sub>3</sub><sup>-</sup> and  
207 HNO<sub>3</sub> concentration using satellite-derived surface NO<sub>2</sub> concentration and their  
208 relationship (Jia et al., 2016). Geddes et al. reconstructed the NO<sub>x</sub> emission data by  
209 using the satellite NO<sub>2</sub> column, and then estimated the global NO<sub>x</sub> deposition by an  
210 ACTM, but the spatial resolution of global NO<sub>x</sub> deposition remains low (2 °×2.5 °),  
211 failing to exploit the higher resolution of satellite observation (Geddes and Martin,  
212 2017).

213 Comparing with NO<sub>2</sub>, the development of satellite NH<sub>3</sub> monitoring is relatively late.  
214 Atmospheric NH<sub>3</sub> was first detected by the TES in Beijing and Los Angeles (Beer et  
215 al., 2008). The IASI sensor also detected atmospheric NH<sub>3</sub> from a biomass burning  
216 event in Greece (Coheur et al., 2009). Subsequently, many scholars began to develop  
217 more reliable satellite NH<sub>3</sub> column retrievals (Whitburn et al., 2016; Van Damme et al.,  
218 2014a), validate the satellite-retrieved NH<sub>3</sub> column with the ground-based observation  
219 (Van Damme et al., 2014a; Dammers et al., 2016; Li et al., 2017), and compare the  
220 satellite NH<sub>3</sub> column with the aircraft measured NH<sub>3</sub> column (Van Damme et al.,  
221 2014b; Whitburn et al., 2016). In recent years, some scholars have carried out the  
222 works of estimating surface NH<sub>3</sub> concentration based on satellite NH<sub>3</sub> column. Liu et  
223 al. obtained the satellite-derived surface NH<sub>3</sub> concentration in China based on the

224 IASI NH<sub>3</sub> column coupled with an ACTM, and deepened the understanding of the  
225 spatial pattern of surface NH<sub>3</sub> concentration in China (Liu et al., 2017b). Similarly,  
226 Graaf et al. carried out the relevant work in Europe based on the IASI NH<sub>3</sub> column  
227 coupled with an ACTM, and estimated the dry NH<sub>3</sub> deposition in West Europe (Van  
228 der Graaf et al., 2018). Jia et al. first constructed the linear model between surface  
229 NO<sub>2</sub> and NH<sub>4</sub><sup>+</sup> concentration based on ground monitoring data, and then calculated  
230 the NH<sub>4</sub><sup>+</sup> concentration using satellite-derived surface NO<sub>2</sub> concentration and their  
231 relationship (Jia et al., 2016). However, as the emission sources of NO<sub>x</sub> (mainly from  
232 transportation and energy sectors) and NH<sub>3</sub> (mainly from agricultural sector) are  
233 different (Hoesly et al., 2018), the linear model between surface NO<sub>2</sub> and NH<sub>4</sub><sup>+</sup>  
234 concentration may lead to large uncertainties in estimating the global NH<sub>4</sub><sup>+</sup>  
235 concentration. There is still no report about the satellite-derived dry and wet reduced  
236 N<sub>r</sub> deposition using satellite NH<sub>3</sub> column at a global scale. As reduced N<sub>r</sub> plays an  
237 important role in total N<sub>r</sub> deposition, satellite NH<sub>3</sub> should be better utilized to help  
238 estimate reduced N<sub>r</sub> deposition.

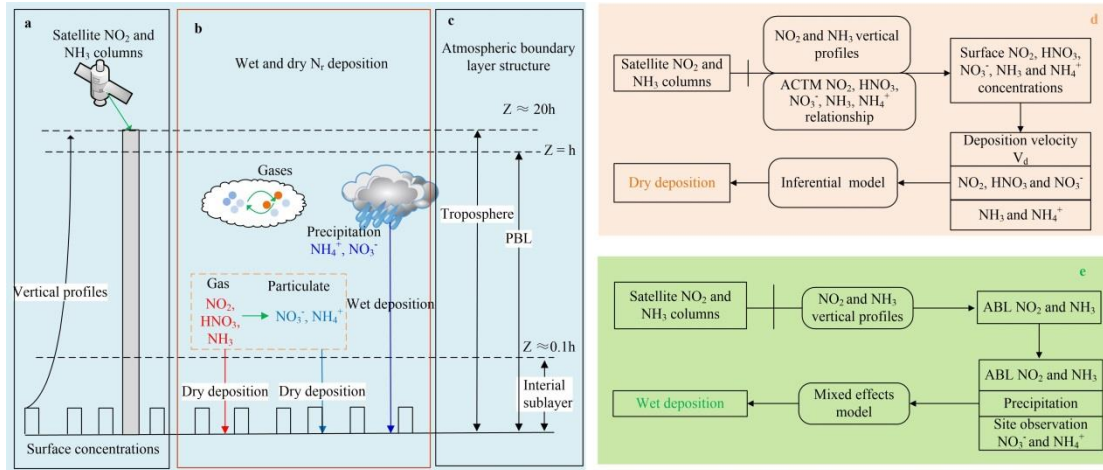
#### 239 **2.4 Problems in Estimating Global N<sub>r</sub> Deposition**

240 The spatial coverage of ground monitoring sites focusing on N<sub>r</sub> deposition is still not  
241 adequate, and the monitoring standards and specifications in different regions of the  
242 world are not consistent, presenting a barrier to integrating different regional  
243 monitoring data. Large uncertainties exist in N<sub>r</sub> emission inventory used to drive the  
244 ACTMs, and the spatial resolution of the modeled N<sub>r</sub> deposition by ACTMs is coarse.  
245 Using satellite monitoring data to estimate surface N<sub>r</sub> concentration and deposition is  
246 still in its infancy, especially for reduced N<sub>r</sub>.  
247 Some scholars tried to use satellite NO<sub>2</sub> and NH<sub>3</sub> column to estimate the surface N<sub>r</sub>  
248 concentration and dry N<sub>r</sub> deposition. However, there are relatively few studies on

249 estimating wet  $N_r$  deposition. In addition, the development of satellite monitoring for  
250  $NH_3$  in the atmosphere is relatively late (compared with  $NO_2$ ). At present, IASI  $NH_3$   
251 data have been widely used, while the effective measurements of TES are less than  
252 IASI; CrIS and AIRS  $NH_3$  column products are still under development. There are  
253 three main concerns in high-resolution estimation of surface  $N_r$  concentration and  
254 deposition based on satellite  $N_r$  observation. (1) How to effectively couple the satellite  
255 high-resolution  $NO_2$  and  $NH_3$  column data with the vertical profiles simulated by an  
256 ACTM, and then estimates the surface  $N_r$  concentrations? This step is the key to  
257 simulate the dry  $N_r$  deposition. (2) How to construct a model for estimating dry  $N_r$   
258 deposition including all major  $N_r$  species based on satellite  $NO_2$  and  $NH_3$  column, and  
259 then estimates the dry  $N_r$  deposition at a high spatial resolution? (3) How to combine  
260 the high-resolution satellite  $NO_2$  and  $NH_3$  column data and ground-based monitoring  
261 data to construct wet  $N_r$  deposition models, and then estimate the wet  $N_r$  deposition at  
262 a high spatial resolution?

### 263 **3. Framework of Estimating Surface $N_r$ Concentration and Deposition Using** 264 **Satellite Observation**

265 Previous studies using satellite observation to estimate surface  $N_r$  concentration and  
266 deposition only focused on one or several  $N_r$  components, but not including all  $N_r$   
267 components, which were decentralized, unsystematic and incomplete. Here we give a  
268 framework of using satellite observation to estimate surface  $N_r$  concentration and  
269 deposition as shown in **Fig. 1** based on recent advances.



270

271 **Fig. 1 Schematic diagram of dry and wet  $N_r$  deposition.** (a) indicates satellite observed  $NO_2$   
 272 and  $NH_3$  column, and the vertical profiles by an ACTM; (b) shows dry and wet  $N_r$  deposition  
 273 including the major  $N_r$  species (gaseous  $NO_2$ ,  $HNO_3$ ,  $NH_3$ , particulate  $NO_3^-$  and  $NH_4^+$ , as well as  
 274 wet  $NO_3^-$  and  $NH_4^+$  in precipitation); (c) illustrates atmospheric vertical structures including the  
 275 troposphere (satellite observation), atmospheric boundary layer (ABL), interfacial sub-layer;  
 276 (d) and (e) represent procedures of calculating the dry and wet  $N_r$  deposition.  
 277

### 278 3.1 Conversion of Satellite $NO_2$ and $NH_3$ Column to Surface $N_r$ Concentration

279 An ACTM can simulate the vertical profiles of  $NO_2$  and  $NH_3$  with multiple layers  
 280 from the surface to the troposphere. For example, the GEOS-Chem ACTM includes  
 281 47 vertical layers from the earth surface to the top of the stratosphere. Most previous  
 282 studies estimated the ratio of surface  $N_r$  concentration (at the first layer) to total  
 283 columns by an ACTM, and then multiply the ratio by satellite columns to estimate  
 284 satellite-derived surface concentration (Geddes et al., 2016; Graaf et al., 2018; Nowlan  
 285 et al., 2014).

286 Another approach tries to fit general vertical profiles of  $NO_2$  and  $NH_3$  (Zhang et al.,  
 287 2017; Liu et al., 2017b; Liu et al., 2017c), and then estimate the ratio of  $N_r$   
 288 concentration at any height to total  $N_r$  columns, and finally multiply the ratio by  
 289 satellite  $NO_2$  and  $NH_3$  columns. This approach has an advantage compared with the  
 290 previous one for that  $NO_2$  and  $NH_3$  concentration at all altitude included in ACTM  
 291 simulations can be estimated. Satellite  $NO_2$  and  $NH_3$  column data had no vertical  
 292 profiles. Surface  $NO_2$  and  $NH_3$  concentration was estimated by modeled  $NO_2$  and

293 NH<sub>3</sub> vertical profiles from the CTM. The Gaussian model was constructed to fit the  
294 multiple layers' NO<sub>2</sub> and NH<sub>3</sub> concentrations with the altitude. The constructed  
295 Gaussian model has general rules, appropriate for converting satellite columns to  
296 surface concentration simply.

297 Taking the estimation of surface NO<sub>2</sub> concentration using the latter approach as an  
298 example, the methods and steps are introduced in the following.

299 Step 1: Calculate the monthly mean NO<sub>2</sub> concentrations at all layers simulated by an  
300 ACTM.

301 Step 2: Construct the vertical profile function of NO<sub>2</sub>. Multiple Gaussian functions are  
302 used to fit the vertical distribution of NO<sub>2</sub> based on the monthly NO<sub>2</sub> concentrations at  
303 all layers calculated in Step 1, in which the independent variable is the height  
304 (altitude), and the dependent variable is NO<sub>2</sub> concentration at a certain height.

305 The basic form of single Gaussian function is (Zhang et al., 2017;Liu et al., 2017b;Liu  
306 et al., 2017c;Whitburn et al., 2016):

$$307 \quad \rho = \rho_{\max} e^{-\left(\frac{Z-Z_0}{\sigma}\right)^2} \quad (1)$$

308 where Z is the height of a layer in the ACTM;  $\rho_{\max}$ ,  $Z_0$  and  $\sigma$  are the maximum NO<sub>2</sub>  
309 concentration, the corresponding height with the maximum NO<sub>2</sub> concentration and the  
310 thickness of NO<sub>2</sub> concentration layer (one standard error of Gaussian function).

311 There are two basic forms of profile shapes of NO<sub>2</sub>: (1) NO<sub>2</sub> concentration reaches the  
312 maximum concentration when reaching a certain height ( $Z_0 \neq 0$ ). As the height  
313 increases, the NO<sub>2</sub> concentration begins to decline; (2) NO<sub>2</sub> concentration is basically  
314 concentrated on the earth surface ( $Z_0 = 0$ ). These two cases are the ideal state of the  
315 vertical distribution of NO<sub>2</sub> concentration. In reality, single Gaussian fitting may not  
316 capture the vertical distribution of NO<sub>2</sub> well. To improve the accuracy of fitting, the  
317 sum of multiple Gaussian functions can be used (Liu et al., 2019):

318  $\rho(Z) = \sum_{i=1}^n \rho_{\max,i} e^{-\left(\frac{Z-Z_{0,i}}{\sigma_i}\right)^2}$  (2)

319 Step 3: Calculate the ratio of NO<sub>2</sub> concentration at the height of h<sub>G</sub> to total columns

320 ( $\int_0^{h_{\text{trop}}} \rho(Z) dx$ ), and then multiply the ratio by satellite column (S<sub>trop</sub>). The

321 satellite-derived N<sub>r</sub> concentration at the height of h<sub>G</sub> can be calculated as:

322  $S_{G\_NO2} = S_{\text{trop}} \times \frac{\rho(h_G)}{\int_0^{h_{\text{trop}}} \rho(Z) dx}$  (3)

323 Step 4: Convert the instantaneous satellite-derived surface NO<sub>2</sub> concentration (S<sub>G\_NO2</sub>)

324 to daily average (S<sub>G\_NO2</sub> \*) using the ratio of average surface NO<sub>2</sub> concentration

325 (G<sub>ACTM</sub><sup>1-24</sup>) to that at satellite overpass time (G<sub>ACTM</sub><sup>overpass</sup>) by an ACTM (Liu et al., 2020):

326  $S_{G\_NO2} * = \frac{G_{\text{ACTM}}^{1-24}}{G_{\text{ACTM}}^{\text{overpass}}} \times S_{G\_NO2}$  (4)

327 The method for estimating the surface NH<sub>3</sub> concentration (S<sub>G\_NH3</sub> \*) is similar to that

328 for estimating the surface NO<sub>2</sub> concentration.

### 329 **3.2 Estimating Surface Concentration of Other N<sub>r</sub> Species**

330 At present, only NO<sub>2</sub> and NH<sub>3</sub> column can be retrieved reliably, and there are no

331 reliable satellite retrievals of HNO<sub>3</sub>, NH<sub>4</sub><sup>+</sup> and NO<sub>3</sub><sup>-</sup>. For example, the IASI HNO<sub>3</sub>

332 product is still in the stage of data development and verification (Ronsmans et al.,

333 2016). Previous studies firstly derive the relationship between N<sub>r</sub> species by an

334 ACTM or by ground-based measurements, and then use the relationship to convert

335 satellite-derived surface NO<sub>2</sub> and NH<sub>3</sub> concentration (S<sub>G\_NH3</sub> \*) to HNO<sub>3</sub>, NH<sub>4</sub><sup>+</sup> and

336 NO<sub>3</sub><sup>-</sup> concentrations:

337 
$$\begin{cases} G_{S\_NO3} = S_{G\_NO2} * \times \frac{G_{\text{ACTM\_NO3}}}{G_{\text{ACTM\_NO2}}} \\ G_{S\_HNO3} = S_{G\_NO2} * \times \frac{G_{\text{ACTM\_HNO3}}}{G_{\text{ACTM\_NO2}}} \\ G_{S\_NH4} = S_{G\_NH3} * \times \frac{G_{\text{ACTM\_NH4}}}{G_{\text{ACTM\_NH3}}} \end{cases}$$
 (5)

338  $\frac{G_{\text{ACTM\_NO3}}}{G_{\text{ACTM\_NO2}}}$ ,  $\frac{G_{\text{ACTM\_HNO3}}}{G_{\text{ACTM\_NO2}}}$ ,  $\frac{G_{\text{ACTM\_NH4}}}{G_{\text{ACTM\_NH3}}}$  is the estimated ratio of between NO<sub>2</sub> and NO<sub>3</sub><sup>-</sup>,

339 NO<sub>2</sub> and HNO<sub>3</sub>, NH<sub>3</sub> and NH<sub>4</sub><sup>+</sup>.

### 340 **3.3 Dry Deposition of N<sub>r</sub>**

341 The resistance of dry N<sub>r</sub> deposition mainly comes from three aspects: aerodynamic  
342 resistance (R<sub>a</sub>), quasi laminar sub-layer resistance (R<sub>b</sub>) and canopy resistance (R<sub>c</sub>).

343 The V<sub>d</sub> can be expressed as

$$344 V_d = \frac{1}{R_a + R_b + R_c} + v_g \quad (6)$$

345 V<sub>g</sub> is gravitational settling velocity. For gases, the V<sub>g</sub> is negligible (V<sub>g</sub>=0).

346 Dry NO<sub>2</sub>, NO<sub>3</sub><sup>-</sup>, HNO<sub>3</sub>, and NH<sub>4</sub><sup>+</sup> deposition can be calculated by:

$$347 F = G_S \times V_d \quad (7)$$

348 Unlike above species, NH<sub>3</sub> is bi-directional, presenting both upward and downward  
349 fluxes. There is a so-called “canopy compensation point” (C<sub>o</sub>) controlling dry NH<sub>3</sub>  
350 deposition. Dry NH<sub>3</sub> deposition can be calculated by:

$$351 F = (G_{S_{NH_3}} - C_o) \times V_d \quad (8)$$

352 The calculation of C<sub>o</sub> is very complex including the leaf stomatal and soil emission  
353 potentials related to the meteorological factors, the plant growth stage and the canopy  
354 type. The satellite-based methods usually neglected this complex process and set C<sub>o</sub>  
355 as zero (Graaf et al., 2018;Kharol et al., 2018) or set fixed values in each land use  
356 type based on ground-based measurements (Jia et al., 2016).

### 357 **3.4 Wet Deposition of N<sub>r</sub>**

358 The satellite-based estimation of wet N<sub>r</sub> deposition can be simplified as the product of  
359 the concentration of N<sub>r</sub> (C), precipitation (P) and scavenging coefficient (w) (Pan et  
360 al., 2012). Satellite NO<sub>2</sub> and NH<sub>3</sub> can be used to indicate the oxidized N<sub>r</sub> and reduced  
361 N<sub>r</sub>; precipitation (P) can be obtained from ground monitoring data or reanalysis data  
362 (such as NCEP). However, the scavenging coefficient (w) is usually highly uncertain.

363 To improve the accuracy of estimation, a mixed-effects model (Liu et al.,

364 2017a;Zhang et al., 2018) is proposed to build the relationship between satellite NO<sub>2</sub>  
365 and NH<sub>3</sub>, precipitation and ground monitoring wet N<sub>r</sub> deposition:

$$366 \text{WetN}_{ij} = \alpha_j + \beta_i \times P_{ij} \times (S_{ABL})_{ij} + \varepsilon_{ij} \quad (9)$$

$$367 S_{ABL} = S_{\text{trop}} \times \frac{\int_0^{\text{ABL}} \rho(Z)dx}{\int_0^{\text{h}_{\text{trop}}} \rho(Z)dx} \quad (10)$$

368 WetN<sub>ij</sub> is wet NO<sub>3</sub><sup>-</sup>N or NH<sub>4</sub><sup>+</sup>-N deposition at month i and site j; (S<sub>ABL</sub>)<sub>ij</sub> is the  
369 atmospheric boundary layer (ABL) NO<sub>2</sub> or NH<sub>3</sub> columns at month i and site j; P<sub>ij</sub> is  
370 precipitation at month i and site j; β<sub>i</sub> and α<sub>j</sub> are the slope and intercept of random  
371 effects, representing seasonal variability and spatial effects; ε<sub>ij</sub> represents the random  
372 error at month i and site j. The mixed effects models were appropriate for estimating  
373 both wet NO<sub>3</sub><sup>-</sup> and NH<sub>4</sub><sup>+</sup> deposition using the satellite observations.

374 The scavenging process of wet N<sub>r</sub> deposition usually starts from the height of rainfall  
375 rather than the top of the troposphere, so it is more reasonable to use NO<sub>2</sub> and NH<sub>3</sub>  
376 column below the height of rainfall to build the wet N<sub>r</sub> deposition model. The NO<sub>2</sub>  
377 and NH<sub>3</sub> column within ABL is used to build the wet deposition model since  
378 precipitation height is close to the height of the ABL (generally less than 2-3 km).

#### 379 **4. Satellite-derived Surface N<sub>r</sub> Concentration and Deposition**

##### 380 **4.1 Surface NO<sub>2</sub> Concentration and Oxidized N<sub>r</sub> Deposition**

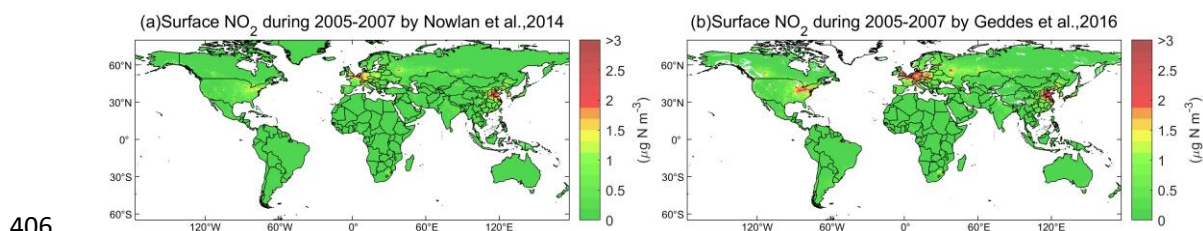
381 The spatial resolutions of global ACTMs and therefore modeled surface N<sub>r</sub>  
382 concentration are very coarse (for example, the spatial resolution of the global version  
383 of GEOS-Chem is 2°×2.5°). Thus it can be hard to estimate surface N<sub>r</sub> concentration  
384 and deposition at a fine resolution at a global scale by ACTMs alone. Instead, the  
385 satellite N<sub>r</sub> retrievals have a high spatial resolution and can reveal more spatial details  
386 than ACTM simulations.

387 Cheng et al. and Jia et al. established a linear model between the surface NO<sub>2</sub>



388 concentration and NO<sub>2</sub> column by assuming the ratio of the surface NO<sub>2</sub>  
389 concentration to the tropospheric NO<sub>2</sub> column to be fixed, and then used the linear  
390 model to convert satellite NO<sub>2</sub> columns to surface NO<sub>2</sub> concentration, and finally  
391 estimated dry NO<sub>2</sub> deposition using the inferential method (Cheng et al., 2013; Jia et  
392 al., 2016). However, these statistical methods are highly dependent on the  
393 ground-based measurements, and the established linear models may be not effective  
394 over regions with few monitoring sites.

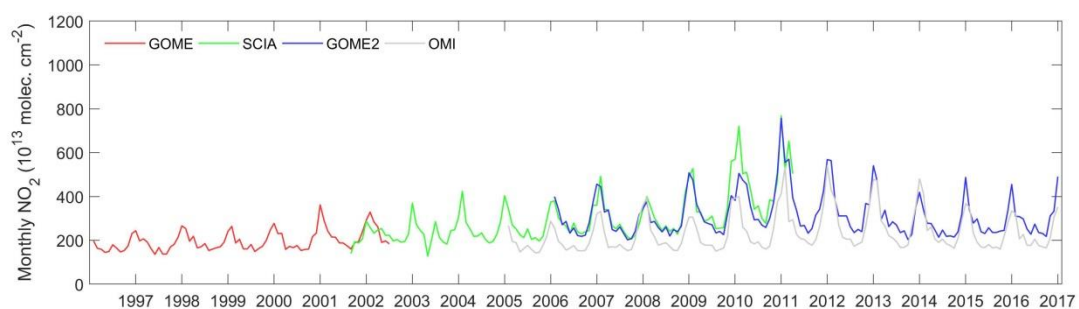
395 A comprehensive study (Nowlan et al., 2014) estimated global surface NO<sub>2</sub>  
396 concentration during 2005-2007 by multiplying OMI tropospheric NO<sub>2</sub> columns by  
397 the ACTM-modeled ratio between surface NO<sub>2</sub> concentration and tropospheric  
398 column (**Fig. 2**). Nowlan et al. also estimated dry NO<sub>2</sub> deposition using the  
399 OMI-derived surface NO<sub>2</sub> concentration combining the modeled V<sub>d</sub> during 2005-2007  
400 (Nowlan et al., 2014). This approach followed an earlier study (Lamsal et al., 2008),  
401 that focus on North America. As reported by Lamsal et al., the satellite-derived  
402 surface NO<sub>2</sub> concentration was generally lower than ground-based NO<sub>2</sub> observations,  
403 ranging from -17% to -36% in North America (Lamsal et al., 2008). Kharol et al. used  
404 a similar method and found the satellite-derived surface NO<sub>2</sub> concentration was only  
405 half of the ground-measured values in North America (Kharol et al., 2015).



407 **Fig. 2** Satellite-derived surface NO<sub>2</sub> concentration during 2005-2007 by Nowlan et al. (Nowlan et  
408 al., 2014) (a) and by Geddes et al. (Geddes et al., 2016) (b). We gained the surface NO<sub>2</sub>  
409 concentration by Nowlan et al. (Nowlan et al., 2014) and by Geddes et al. (Geddes et al., 2016) at  
410 the web: [http://fizz.phys.dal.ca/~atmos/martin/?page\\_id=232](http://fizz.phys.dal.ca/~atmos/martin/?page_id=232).

411  
412 Geddes et al. followed previous studies, and used NO<sub>2</sub> column from the GOME,  
413 SCIAMACHY, and GOME-2 to estimate surface NO<sub>2</sub> concentration (Geddes et al.,

414 2016). Although Geddes et al. did not evaluate their results with ground-based  
415 observation (Geddes et al., 2016), it is obvious that their surface NO<sub>2</sub> estimates were  
416 higher than Nowlan's estimates based on OMI (Nowlan et al., 2014) (**Fig. 2**). This  
417 may be because the OMI-derived NO<sub>2</sub> column is much lower than that derived by  
418 GOME, SCIAMACHY, and GOME-2, especially over polluted regions. For example,  
419 in China, the OMI NO<sub>2</sub> column is about 30% lower than that of SCIAMACHY and  
420 GOME-2 consistently (**Fig. 3**).



421

422 **Fig. 3** An example of the time series of monthly NO<sub>2</sub> column retrieved by GOME, SCIAMACHY,  
423 GOME2 and OMI in China. We obtained the GOME, SCIAMACHY, GOME2 and OMI data from  
424 <http://www.temis.nl/airpollution/no2.html>.

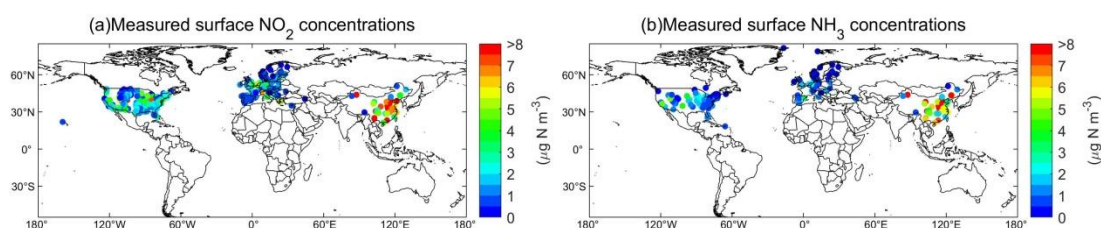
425

426 Larkin et al. established a land-use regression model to estimate global surface NO<sub>2</sub>  
427 concentration by combining satellite-derived surface NO<sub>2</sub> concentration by Geddes et  
428 al. and ground-based annual NO<sub>2</sub> measurements (Geddes et al., 2016;Larkin et al.,  
429 2017). The study by Larkin et al. can be considered as using the ground-based annual  
430 measurements to adjust the satellite-derived surface NO<sub>2</sub> concentration by Geddes et  
431 al. (Geddes et al., 2016;Larkin et al., 2017), which helped reduce the discrepancy  
432 between satellite-derived and ground-measured NO<sub>2</sub> concentration. The regression  
433 model captured 54% of global NO<sub>2</sub> variation, with an absolute error of 2.32 μg N m<sup>-3</sup>.  
434 Zhang et al. followed the framework in **Sect. 3** to estimate the OMI-derived surface  
435 NO<sub>2</sub> concentration (at ~50 m) in China, and found good agreement with ground-based  
436 surface NO<sub>2</sub> concentration from the NNDMN at yearly scale (slope=1.00, R<sup>2</sup>=0.89)  
437 (Zhang et al., 2017). The methods by Zhang et al. can also generate OMI-derived NO<sub>2</sub>

438 concentration at any height by the constructed NO<sub>2</sub> vertical profile (Zhang et al.,  
439 2017). Zhang et al. also estimated dry NO<sub>2</sub> deposition using the OMI-derived surface  
440 NO<sub>2</sub> concentration combining the modeled V<sub>d</sub> during 2005-2016 (Zhang et al., 2017).  
441 Based on Zhang's estimates, the Gaussian function can well simulate the vertical  
442 distribution of NO<sub>2</sub> from an ACTM (MOZART) (Emmons et al., 2010) with 99.64%  
443 of the grids having R<sup>2</sup> values higher than 0.99. This suggests that the  
444 ACTM-simulated vertical distribution of NO<sub>2</sub> has a general pattern, which can be  
445 emulated by Gaussian functions. Once a vertical profile was constructed, it can be  
446 easily used to estimate NO<sub>2</sub> concentration at any height.

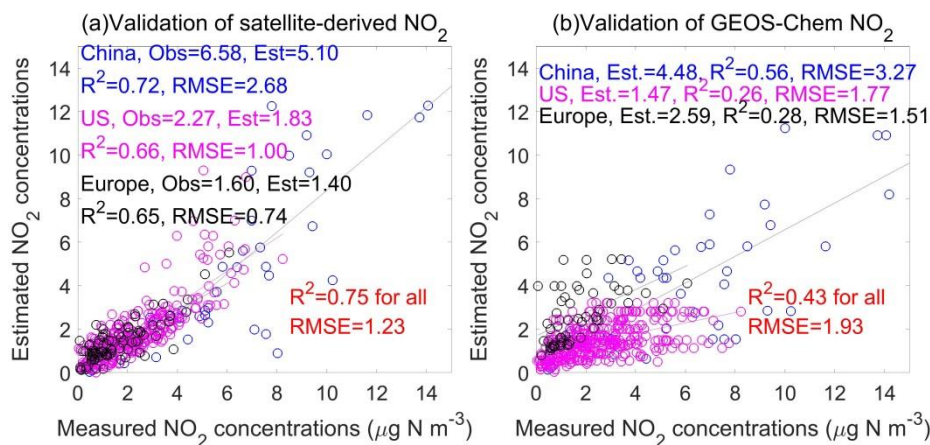
447 In this study, we used the framework in **Sect. 3** to estimate the OMI-derived surface  
448 NO<sub>2</sub> concentration globally. To validate the OMI-derived surface NO<sub>2</sub> concentrations,  
449 ground-measured surface NO<sub>2</sub> concentration in China, the US and Europe in 2014  
450 was collected (**Fig. 4**). The total number of NO<sub>2</sub> observations in China, the US and  
451 Europe are 43, 373 and 88 respectively. The OMI-derived annual average for all sites  
452 was 3.74 μg N m<sup>-3</sup>, which was close to the measured average (3.06 μg N m<sup>-3</sup>). The R<sup>2</sup>  
453 between OMI-derived surface NO<sub>2</sub> concentrations and ground-based NO<sub>2</sub>  
454 measurements was 0.75 and the RMSE was 1.23 μg N m<sup>-3</sup> (**Fig. 5**), which is better  
455 than the modeling results by the GEOS-Chem ACTM (R<sup>2</sup>=0.43, RMSE=1.93 μg N  
456 m<sup>-3</sup>). We did not simply use the relationship between the NO<sub>2</sub> column and surface  
457 NO<sub>2</sub> concentration from the CTM. As presented in the methods, we can estimate  
458 surface NO<sub>2</sub> concentration at any height by using the Gaussian function. We used the  
459 surface NO<sub>2</sub> concentration at a certain height (~60 m) which best matched with the  
460 ground-based measurements. Satellite-based methods have the advantages of  
461 spatiotemporally continuous monitoring N<sub>r</sub> at a higher resolution, which helps  
462 alleviate the problem of the coarse resolution of ACTMs in estimating N<sub>r</sub>

463 concentration and deposition. The readers can use any satellite data (GOME,  
 464 SCIAMACHY, GOME2 or OMI) combining the Gaussian function to estimate  
 465 surface NO<sub>2</sub> concentrations. They can use surface NO<sub>2</sub> concentrations at a certain  
 466 height which best matched with the ground-based measurements. The key is not  
 467 selecting which satellite data we should use, but determining which height of surface  
 468 NO<sub>2</sub> concentrations that better matched with the ground-based measurements by  
 469 Gaussian function.



470

471 **Fig. 4** Spatial distribution of measured surface NO<sub>2</sub> and NH<sub>3</sub> concentrations in 2014. For NO<sub>2</sub> (a),  
 472 the measured data in China, the US and Europe were obtained from the NNDMN, US-EPA and  
 473 EMEP, respectively; for NH<sub>3</sub> (b), the measured data in China, the US and Europe were obtained  
 474 from the NNDMN, US-AMoN and EMEP, respectively  
 475

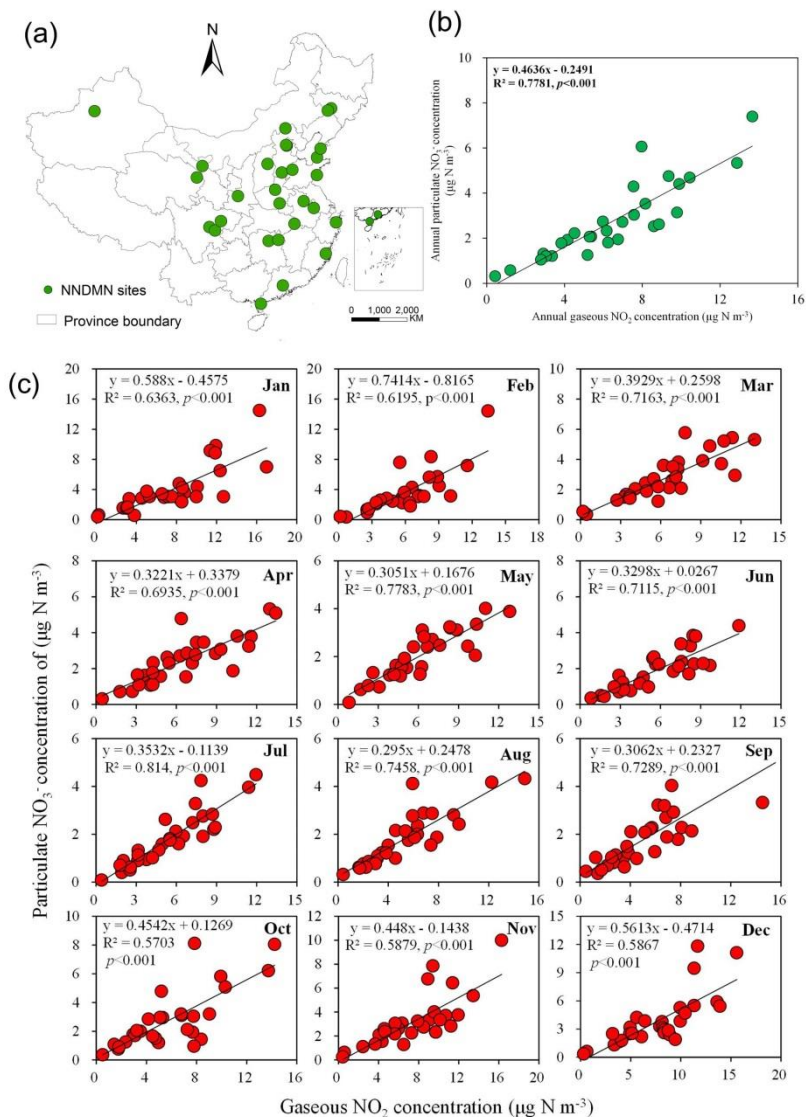


476

477 **Fig. 5** Comparison between annual mean satellite-derived and ground-measured surface NO<sub>2</sub>  
 478 concentrations (a), and comparison between annual mean modeled (by an ACTM as GEOS-Chem)  
 479 and ground-measured surface NO<sub>2</sub> concentrations (b). The ground-based monitoring sites are  
 480 shown in **Fig. 4**.  
 481

482 For NO<sub>3</sub><sup>-</sup> and HNO<sub>3</sub>, previous studies firstly constructed the relationship between NO<sub>2</sub>,  
 483 NO<sub>3</sub><sup>-</sup> and HNO<sub>3</sub>, and found a relatively high linear relationship between NO<sub>2</sub>, NO<sub>3</sub><sup>-</sup>,  
 484 and HNO<sub>3</sub> at a monthly or yearly scale. For example, Jia et al. found a linear

485 relationship between  $\text{NO}_2$  and  $\text{NO}_3^-$ ,  $\text{HNO}_3$  concentration at annual scale ( $R^2=0.70$ )  
486 (Jia et al., 2016). Similarly, based on the ground-based measurements in the NNDMN,  
487 a high correlation was found between surface  $\text{NO}_2$  and  $\text{NO}_3^-$  concentration at monthly  
488 or annual timescales (**Fig. 6**) (Liu et al., 2017c). Using these linear relationships and  
489 satellite-derived surface  $\text{NO}_2$  concentration, the annual mean surface  $\text{NO}_3^-$  and  $\text{HNO}_3$   
490 can be estimated. Alternatively, the relationship of  $\text{NO}_2$ ,  $\text{NO}_3^-$  and  $\text{HNO}_3$  can also be  
491 modeled by an ACTM. For example, a strong relationship of tropospheric  $\text{NO}_2$ ,  $\text{NO}_3^-$   
492 and  $\text{HNO}_3$  column was simulated over all months by an ACTM, with the correlation  
493 ranging from 0.69 to 0.91 (Liu et al., 2017a). But, over shorter timescales, the  
494 relationship between  $\text{NO}_2$ ,  $\text{NO}_3^-$  and  $\text{HNO}_3$  may be nonlinear, which we should be  
495 cautious about when estimating surface  $\text{NO}_3^-$  and  $\text{HNO}_3$  concentration from  $\text{NO}_2$   
496 concentration.



497

498 **Fig. 6** Correlation between surface NO<sub>2</sub> and particulate NO<sub>3</sub><sup>-</sup> concentration in the NNDMN at  
 499 annual and monthly scales, which were adopted from our previous study (Liu et al., 2017c). (a)  
 500 indicates the spatial locations of monitoring sites in the NNDMN; (b) and (c) represent yearly and  
 501 monthly relationship between surface NO<sub>2</sub> and particulate NO<sub>3</sub><sup>-</sup> concentration, respectively.  
 502

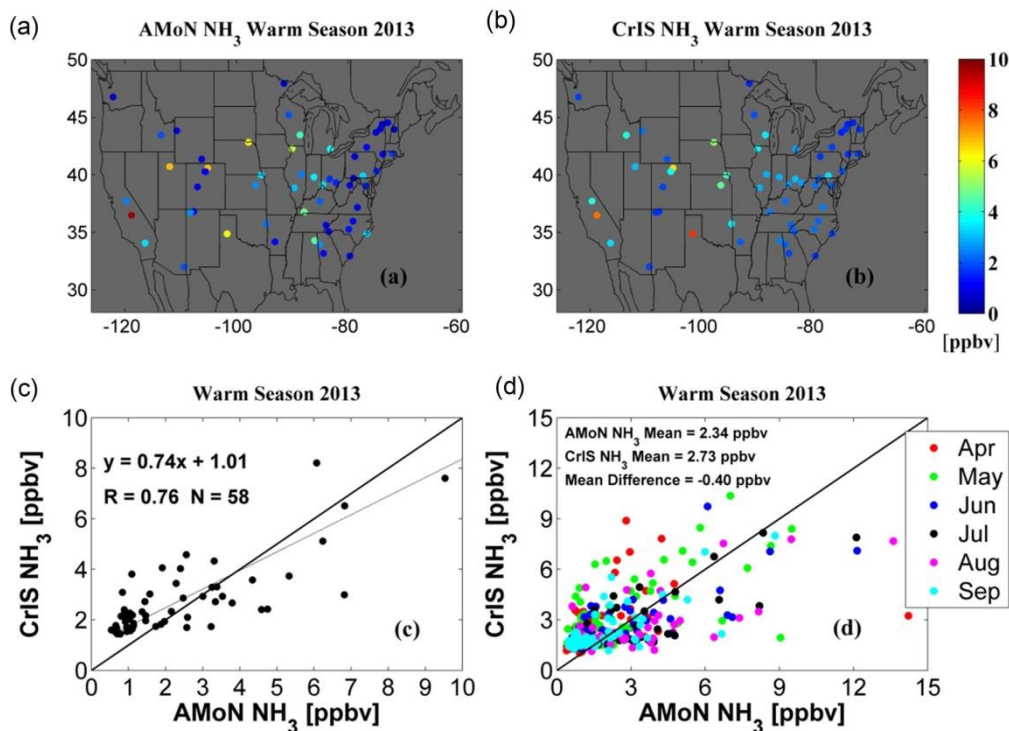
503 For the wet N<sub>r</sub> deposition, Liu et al. followed the framework in **Sect. 3** to estimate wet  
 504 nitrate deposition using ABL NO<sub>2</sub> columns derived from OMI NO<sub>2</sub> column and NO<sub>2</sub>  
 505 vertical profile from an ACTM (MOZART), and precipitation by a mixed-effects  
 506 model showing the proposed model can achieve high predictive power for monthly  
 507 wet nitrate deposition over China (R=0.83, RMSE=0.72) (Liu et al., 2017a).

## 508 4.2 Surface NH<sub>3</sub> Concentration and Reduced N<sub>r</sub> Deposition

509 With the development of atmospheric remote sensing of NH<sub>3</sub>, some scholars have

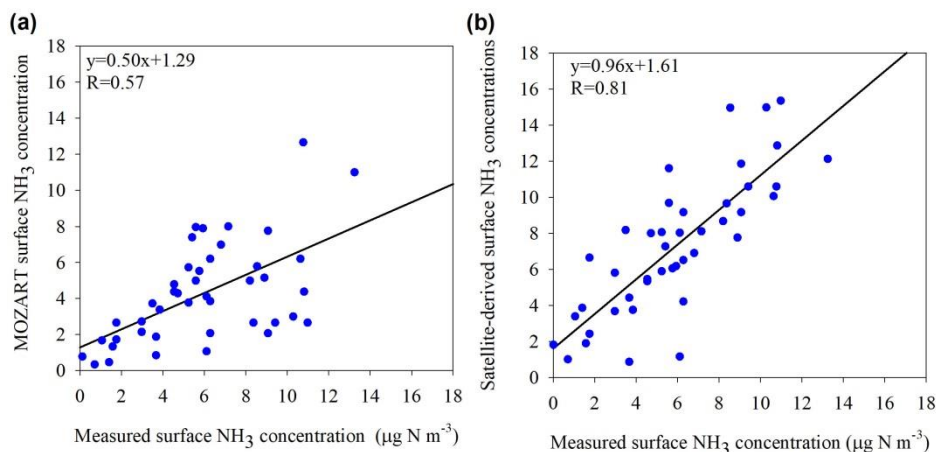
510 estimated surface  $\text{NH}_3$  concentration and dry  $\text{NH}_3$  deposition based on the satellite  
511  $\text{NH}_3$  column data. Assuming the ratio between the surface  $\text{NH}_3$  concentration to the  
512  $\text{NH}_3$  column was fixed, Yu et al. applied a linear model to convert satellite  $\text{NH}_3$   
513 columns to surface  $\text{NH}_3$  concentration and estimated dry  $\text{NH}_3$  deposition in China  
514 using the inferential method (Yu et al., 2019). But Yu et al. did not consider the spatial  
515 variability of the vertical profiles of  $\text{NH}_3$  (Yu et al., 2019), which may cause a large  
516 uncertainty in estimating surface  $\text{NH}_3$  concentration.

517 In Western Europe, Graaf et al. used the ratio of the surface  $\text{NH}_3$  concentration (in the  
518 bottom layer) to total  $\text{NH}_3$  column from an ACTM to convert the IASI  $\text{NH}_3$  column to  
519 surface  $\text{NH}_3$  concentration, and then estimated dry  $\text{NH}_3$  deposition combining the  
520 modeled deposition velocity and IASI-derived surface  $\text{NH}_3$  concentration (Graaf et al.,  
521 2018). Similarly, in North America, Kharol et al. estimated the dry  $\text{NH}_3$  deposition by  
522 the CrIS-derived surface  $\text{NH}_3$  concentration and deposition velocity of  $\text{NH}_3$  (Kharol et  
523 al., 2018). They found a relatively high correlation ( $R=0.76$ ) between the  
524 CrIS-derived surface  $\text{NH}_3$  concentration and AMoN measurements during warm  
525 seasons (from April to September) in 2013 (**Fig. 7**). Over China, Liu et al. found a  
526 higher correlation ( $R=0.81$ ) between IASI-derived surface  $\text{NH}_3$  concentrations and the  
527 measured surface  $\text{NH}_3$  concentrations than those from an ACTM ( $R=0.57$ , **Fig. 8**)  
528 (Liu et al., 2017b).



529

530 **Fig. 7** Comparisons of the measured surface  $\text{NH}_3$  concentration by the AMoN and CrIS-derived  
 531 surface  $\text{NH}_3$  concentration in the US during warm season (April-September) in 2013 (Kharol et al.,  
 532 2018). (a) and (b) indicate measured and CrIS-derived surface  $\text{NH}_3$  concentration at the AMoN  
 533 sites, respectively; (c) represents the comparison of averaged surface  $\text{NH}_3$  concentration during  
 534 warm months between CrIS-derived estimates and measurements, while (d) indicates the  
 535 comparison of monthly surface  $\text{NH}_3$  concentration between CrIS-derived estimates and  
 536 measurements.  
 537



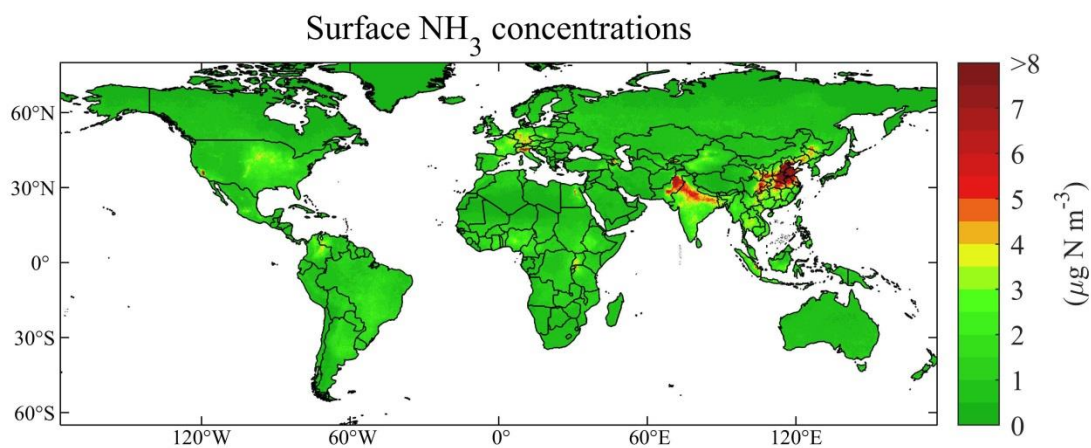
538

539 **Fig. 8** Comparisons of the measured surface  $\text{NH}_3$  concentration with IASI-derived surface  $\text{NH}_3$   
 540 concentration at the NNDMN sites over China (Liu et al., 2017b). (a) indicates the comparison of  
 541 measured and modeled surface  $\text{NH}_3$  concentration from an ACTM (MOZART), and (b) represents  
 542 the comparison of the measured and IASI-derived surface  $\text{NH}_3$  concentration.  
 543

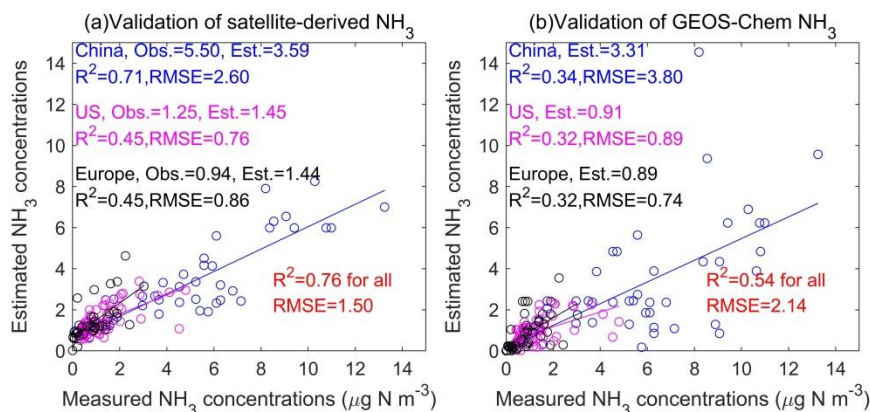
544 Liu et al. followed the framework in **Sect. 3** to estimate the IASI-derived surface  $\text{NH}_3$   
 545 concentration (at the middle height of the first layer by an ACTM) (**Fig. 9**), and found



546 a good agreement with ground-based surface NH<sub>3</sub> concentration (Liu et al., 2019).  
547 The correlation between the measured and satellite-derived annual mean surface NH<sub>3</sub>  
548 concentrations over all sites was 0.87 as shown in **Fig. 10**, while the average  
549 satellite-derived and ground-measured surface NH<sub>3</sub> concentration was 2.52 and 2.51  
550  $\mu\text{g N m}^{-3}$  in 2014 at the monitoring sites, respectively. The satellite-derived estimates  
551 achieved a better accuracy ( $R^2=0.76$ ,  $\text{RMSE} = 1.50 \mu\text{g N m}^{-3}$ ) than an ACTM  
552 (GEOS-Chem,  $R^2=0.54$ ,  $\text{RMSE} = 2.14 \mu\text{g N m}^{-3}$ ). The satellite NH<sub>3</sub> retrievals were  
553 affected by the detection limits of the satellite instruments and thermal contrast.  
554 Higher correlation over China than other regions for the satellite estimates was linked  
555 to the detection limits by the instruments and thermal contrast (Liu et al., 2019).  
556 Higher accuracy could be gained with higher thermal contrast and NH<sub>3</sub> abundance.  
557 Instead, the uncertainties of NH<sub>3</sub> retrievals would be higher with lower thermal  
558 contrast and NH<sub>3</sub> abundance.



560 **Fig. 9** Spatially satellite-based surface NH<sub>3</sub> estimates in 2014 (Liu et al., 2019). The global surface  
561 NH<sub>3</sub> concentration datasets have been released on the website:  
562 <https://zenodo.org/record/3546517#.Xj6I4GgzY2w>.  
563

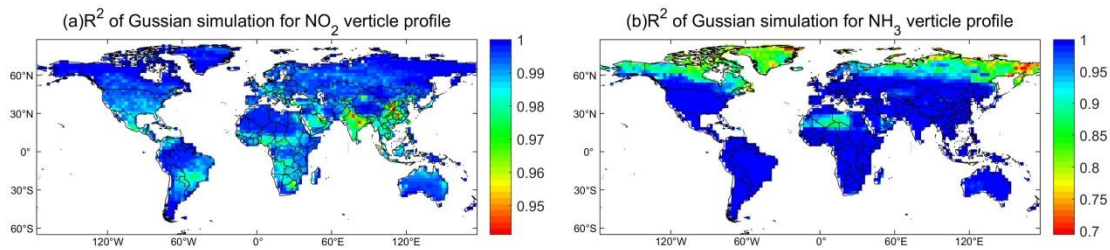


564

565 **Fig. 10** Comparison between yearly satellite-based and measured surface NH<sub>3</sub> concentrations (a),  
 566 and comparison between yearly modeling (by an ACTM as GEOS-Chem) and measured surface  
 567 NH<sub>3</sub> concentrations (b) (Liu et al., 2019). The ground-based monitoring sites are shown in **Fig. 4**.  
 568

569 The proposed methods (Liu et al., 2019) can also estimate NH<sub>3</sub> concentration at any  
 570 height using the constructed vertical profile function of NH<sub>3</sub>. The Gaussian function  
 571 can well emulate the vertical distribution of NH<sub>3</sub> from an ACTM outputs with 99% of  
 572 the grids having R<sup>2</sup> values higher than 0.90 (**Fig. 11**). This means, for regional and  
 573 global estimation, the vertical distribution of NH<sub>3</sub> concentration has a general pattern,  
 574 which can be mostly emulated by the Gaussian function. Once a global NH<sub>3</sub> vertical  
 575 profile was simulated, it can be easily used to estimate satellite-derived NH<sub>3</sub>  
 576 concentration at any height. We can also estimate dry NH<sub>3</sub> deposition using the  
 577 IASI-derived surface NH<sub>3</sub> concentration combining the modeled V<sub>d</sub>. For the dry  
 578 deposition, the uncertainty mainly came from the satellite-derived estimates using the  
 579 modeled vertical profiles. The uncertainty of vertical profiles modeled by the ACTM  
 580 mainly resulted from the chemical and transport mechanisms. We recommend using  
 581 the Gaussian function to determine the height of surface NO<sub>2</sub> and NH<sub>3</sub> concentrations  
 582 that best matched with the ground-based measurements. There may exist systematic  
 583 biases by simply using the relationship of NO<sub>2</sub> columns and surface concentration to  
 584 estimate satellite surface NO<sub>2</sub> concentrations. To date, there are still no studies

585 developing satellite-based methods to estimate the wet reduced  $N_r$  deposition on a  
586 regional scale.



587

588 **Fig. 11** Spatial distributions of  $R^2$  for Gaussian function by simulating  $NH_3$  and  $NO_2$  vertical  
589 profiles. This is an example of Gaussian fitting using 47 layers'  $NH_3$  and  $NO_2$  concentration from  
590 an ACTM (GEOS-Chem).  
591

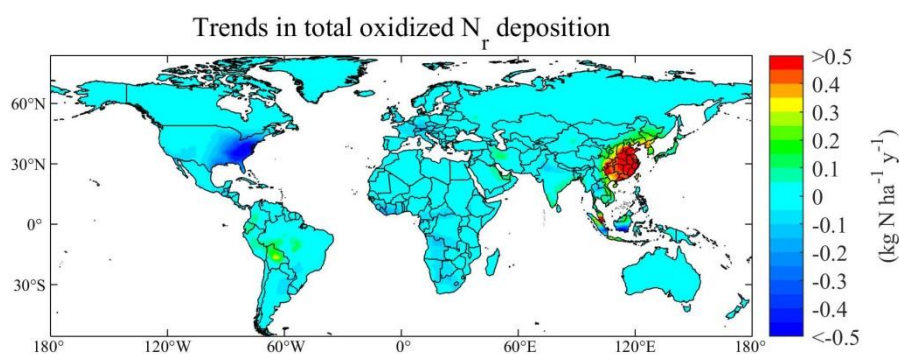
## 592 **5. Trends of Surface $N_r$ Concentration and Deposition by Satellite-based**

### 593 **Methods**

594 The  $N_r$  concentration and deposition modeled by ACTMs are highly dependent on the  
595 accuracy of input  $N_r$  emissions. The methods commonly used to estimate  
596 anthropogenic  $N_r$  emissions are based on the data of human activities and emission  
597 factors, which can be highly uncertain. The ACTM methods driven by  $N_r$  emission  
598 inventory have relatively poor timeliness, and have limitations in monitoring the  
599 recent trends of  $N_r$  deposition.

600 Satellite-based methods provide a simple, fast and relatively objective way to  
601 monitoring  $N_r$  deposition at a high resolution, and less susceptible to the errors in the  
602 assumptions that emission inventories are compiled based on, particularly the lack of  
603 reliable data over developing countries (Crippa et al., 2018). With such advantages,  
604 researchers developed the satellite-based methods to estimate surface  $N_r$  concentration,  
605 deposition and even emissions. Satellite-based methods have advantages in  
606 monitoring the recent trends of  $N_r$  deposition. Geddes et al. used  $NO_2$  column from  
607 the GOME, SCIAMACHY, and GOME-2 to estimate satellite-derived  $NO_x$  emissions,  
608 and then used the calibrated  $NO_x$  emission inventory to drive an ACTM to simulate  
609 the long-term oxidized  $N_r$  deposition globally (Geddes and Martin, 2017). They found

610 oxidized  $N_r$  deposition from 1996 to 2014 decreased by 60% in Eastern US, doubled  
611 in East China, and declined by 20% in Western Europe (**Fig. 12**). We use the datasets  
612 by Geddes et al. to calculate the trends of total oxidized  $N_r$  deposition during  
613 1996-2014 (Geddes and Martin, 2017). It is obvious that two completely opposite  
614 trends exist: (1) in East China with a steep increase of higher than  $0.5 \text{ kg N ha}^{-1} \text{ y}^{-1}$   
615 and (2) East US with a steep decrease of lower than  $-0.5 \text{ kg N ha}^{-1} \text{ y}^{-1}$ . Although it is  
616 not a direct way to use satellite  $N_r$  observation to estimate  $N_r$  deposition, the method  
617 of estimating trends of  $N_r$  deposition by Geddes et al. can be considered effective  
618 since it took account of the changes of both  $\text{NO}_x$  emission and climate by an ACTM  
619 (Geddes and Martin, 2017).



620

621 **Fig. 12** Gridded annual changes of total oxidized  $N_r$  deposition simulated by GEOS-Chem  
622 constrained with GOME, SCIAMACHY, and GOME-2  $\text{NO}_2$  retrievals during 1996-2014 (Geddes  
623 and Martin, 2017). We gained the generated datasets  
624 ([http://fizz.phys.dal.ca/~atmos/martin/?page\\_id=1520](http://fizz.phys.dal.ca/~atmos/martin/?page_id=1520)) by Geddes et al., and calculated the trends  
625 using the linear methods.  
626

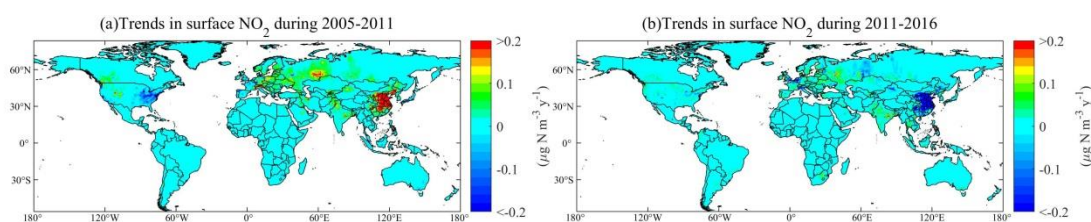
627 Some researchers developed a more direct way to infer the trends of surface  $N_r$   
628 concentration and deposition. Geddes et al. presented a comprehensive long-term  
629 global surface  $\text{NO}_2$  concentration estimate (at  $0.1^\circ$  resolution using an oversampling  
630 approach) between 1996 and 2012 by using  $\text{NO}_2$  column from the GOME,  
631 SCIAMACHY, and GOME-2 (Geddes et al., 2016). The surface  $\text{NO}_2$  concentration in  
632 North America (the US and Canada) decreased steeply, followed by Western Europe,  
633 Japan and South Korea, while approximately tripled in China and North Korea

634 (Geddes et al., 2016). Jia et al. established a simple linear regression model based on  
635 OMI NO<sub>2</sub> column and ground-based surface N<sub>r</sub> concentration, and then estimated the  
636 trends of dry N<sub>r</sub> deposition globally between 2005 and 2014 (Jia et al., 2016). They  
637 found that dry N<sub>r</sub> deposition in Eastern China increased rapidly, while in the Eastern  
638 US, Western Europe, and Japan dry N<sub>r</sub> deposition has decreased in recent decades.

639 We used the proposed framework to estimate the long-term surface NO<sub>2</sub>  
640 concentrations by OMI during 2005-2016. Note that the simulated profile function has  
641 a general rule, which can be well simulated by Gaussian function for any year (for our  
642 case during 2005-2016). The emission inventories should not affect the vertical  
643 profiles shapes using Gaussian function, but the transport and chemical mechanism in  
644 the CTM may affect the accuracy of the vertical profile distribution. The  
645 satellite-based methods did not need to rely on the accuracy of the statistical emission  
646 data. We split the time span of 2005-2016 into two periods: 2005-2011 and 2011-2016,  
647 as surface NO<sub>2</sub> concentration shows opposite trend in China in these two periods. The  
648 magnitudes of both growth and decline in surface NO<sub>2</sub> concentration in China are  
649 most pronounced worldwide in the two periods (**Fig. 13**). During 2005-2011, apart  
650 from Eastern China with the largest increase in surface NO<sub>2</sub> concentration, there are  
651 also several areas with increasing trends such as Northwest and East India (New Delhi  
652 and Orissa), Western Russia, Eastern Europe (Northern Italy), Western US (Colorado  
653 and Utah), Northwestern US (Seattle and Portland), Southwestern Canada (Vancouver,  
654 Edmonton, Calgary), Northeast Pakistan and Northwest Xinjiang (Urumqi). Notably,  
655 the biggest decreases in surface NO<sub>2</sub> concentration during 2005-2011 occurred in  
656 Eastern US and Western EU (North France, South England, and West German).

657 During 2011-2016, due to the strict control of NO<sub>x</sub> emissions, Eastern China had the  
658 largest decrease in surface NO<sub>2</sub> concentration than elsewhere worldwide, followed by

659 Western Xinjiang, Western Europe and some areas in Western Russia.

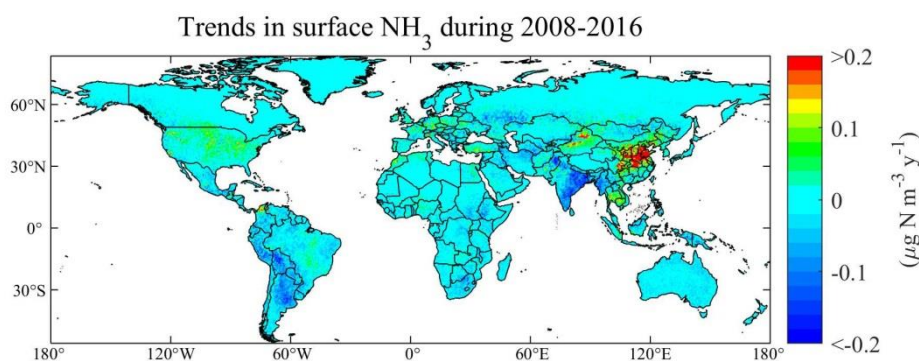


660

661 **Fig. 13** Gridded annual changes in surface  $\text{NO}_2$  concentrations gained by OMI retrievals during  
662 2005-2011 (a) and during 2011-2016 (b) in this study. We have released the global surface  $\text{NO}_2$   
663 concentrations during 2005-2016 available at the website:  
664 <https://zenodo.org/record/3546517#.Xj6I4GgzY2w>.

665

666 Liu et al. estimated surface  $\text{NH}_3$  concentration globally during 2008-2016 using  
667 satellite  $\text{NH}_3$  retrievals by IASI (Liu et al., 2019). A large increase of surface  $\text{NH}_3$   
668 concentrations was found in Eastern China, followed by Northern Xinjiang province  
669 in China during 2008-2016 (**Fig. 14**). Satellite-based methods have been proven as an  
670 effective and unique way to monitoring the trends of global  $\text{N}_r$  concentration and  
671 deposition. To date, there are still few studies reporting the satellite-derived trends of  
672 reduced  $\text{N}_r$  deposition on a global scale.



673

674 **Fig. 14** Gridded annual changes in surface  $\text{NH}_3$  concentrations gained by IASI retrievals during  
675 2008-2016 (Liu et al., 2019). We have released the global surface  $\text{NH}_3$  concentrations during  
676 2008-2016 at the website: <https://zenodo.org/record/3546517#.Xj6I4GgzY2w>.

677

## 678 6. Remaining Challenges for Estimating $\text{N}_r$ Deposition Using Satellite

### 679 Observation

680 First, the reduced  $\text{N}_r$  deposition plays an important contribution to total  $\text{N}_r$  deposition.

681  $\text{NH}_3$  exhibits bi-directional air-surface exchanges. The  $\text{NH}_3$  compensation point

682 (Farquhar et al., 1980) is also an important and highly variable factor controlling dry  
683  $\text{NH}_3$  deposition (Schrader et al., 2016; Zhang et al., 2010). However, the current  
684 existing satellite-based methods did not consider this bi-directional air-surface  
685 exchange. It is important to better parameterize the  $\text{NH}_3$  compensation point, and  
686 assess the effects of bi-directional air-surface exchanges on estimating the dry  $\text{NH}_3$   
687 deposition.

688 Second, the existing satellite-based methods to estimate  $\text{N}_r$  deposition used the ratio  
689 of the surface  $\text{N}_r$  concentration to the  $\text{N}_r$  column by an ACTM to convert satellite  $\text{N}_r$   
690 column to surface  $\text{N}_r$  concentration. However, the calculated ratio (by an ACTM) and  
691 the satellite  $\text{N}_r$  column have different spatial resolutions, and previous studies usually  
692 applied the modeled ratio directly or interpolate the ratio into the resolution of  
693 satellite  $\text{N}_r$  column. This method assumes the relationship at coarse resolution by an  
694 ACTM can also be effective in fine resolution as satellite indicated. When regional  
695 studies are conducted, regional ACTMs coupled with another meteorological model  
696 (e.g. WRF-Chem, WRF-CMAQ) (Grell et al., 2005; Wong et al., 2012) can be  
697 configured to match the spatial resolution of satellite observation, but this is not as  
698 viable for global ACTMs (e.g. MOZART, GEOS-Chem) due to differences in model  
699 structures and computational cost. The modeled ratio of surface  $\text{N}_r$  concentration to  
700 the  $\text{N}_r$  column may have variability at spatial scales finer than the horizontal  
701 resolution of global ACTMs. The impact of such scale effect (at different spatial  
702 scales) on estimated surface  $\text{N}_r$  concentration should be further studied.

703 Third, the satellite observation can only obtain reliable  $\text{NO}_2$  and  $\text{NH}_3$  column  
704 presently, and there are no available high-resolution and reliable direct  $\text{HNO}_3$ ,  $\text{NO}_3^-$ ,  
705  $\text{NH}_4^+$  retrievals. For  $\text{HNO}_3$ ,  $\text{NO}_3^-$ ,  $\text{NH}_4^+$  concentrations, the satellite-based methods  
706 often applied the satellite-derived  $\text{NO}_2$  and  $\text{NH}_3$  concentration and the relationship

707 between  $N_r$  species from an ACTM (or ground-based measurements) to estimate  
708 surface  $HNO_3$ ,  $NO_3^-$ ,  $NH_4^+$  concentration. With the development of satellite  
709 technology, more and more  $N_r$  species can be detected, such as  $HNO_3$ . However, at  
710 present, satellite  $HNO_3$  products are not mature, and the spatial resolution is low.  
711 Direct, high-resolution and reliable satellite monitoring of more  $N_r$  species is critical  
712 to further developing the use of using atmospheric remote sensing to estimate  $N_r$   
713 deposition at global and regional scales.

714 Fourth, estimating wet  $N_r$  deposition using satellite  $NO_2$  and  $NH_3$  column remains  
715 relatively uncommon. Further studies should focus on how to combine the  
716 high-resolution satellite  $NO_2$  and  $NH_3$  column and the ground-based monitoring data  
717 to build wet  $N_r$  deposition models to estimate wet  $N_r$  deposition at higher  
718 spatiotemporal resolution. The proposed scheme to estimate the wet  $N_r$  deposition in  
719 **Sect. 3** is statistical. As far as we know, previous studies using satellite  $NO_2$  and  $NH_3$   
720 column to estimate wet  $N_r$  deposition were through a statistical way, and no studies  
721 were done from a mechanism perspective. The wet  $N_r$  deposition includes the  
722 scavenging processes of in-cloud, under-cloud and precipitation. Processed-level  
723 knowledge and models can benefit the estimation of wet  $N_r$  deposition using satellite  
724  $NO_2$  and  $NH_3$  column.

## 725 **7. Conclusion**

726 The recent advances of satellite-based methods for estimating surface  $N_r$   
727 concentration and deposition have been reviewed. Previous studies have focused on  
728 using satellite  $NO_2$  column to estimate surface  $NO_2$  concentrations and dry  $NO_2$   
729 deposition both regionally and globally. The research on calculating surface  $NH_3$   
730 concentration and reduced  $N_r$  deposition by satellite  $NH_3$  data is just beginning, and  
731 some scholars have carried out estimating surface  $NH_3$  concentration and dry  $NH_3$



732 deposition on different spatial and temporal scales, but the research degree is still  
733 relatively low. We present a framework of using satellite NO<sub>2</sub> and NH<sub>3</sub> column to  
734 estimate N<sub>r</sub> deposition based on recent advances. The proposed framework of using  
735 Gaussian function to model vertical NO<sub>2</sub> and NH<sub>3</sub> profiles can be used to convert the  
736 satellite NO<sub>2</sub> and NH<sub>3</sub> column to surface NO<sub>2</sub> and NH<sub>3</sub> concentration at any height  
737 simply and quickly. The proposed framework of using satellite NO<sub>2</sub> and NH<sub>3</sub> column  
738 to estimate wet N<sub>r</sub> deposition is a statistical way, and further studies should be done  
739 from a mechanism perspective. Finally, we summarized current challenges of using  
740 satellite NO<sub>2</sub> and NH<sub>3</sub> column to estimate surface N<sub>r</sub> concentration and deposition  
741 including a lack of considering NH<sub>3</sub> bidirectional air-surface exchanges and the  
742 problem of different spatial scales between an ACTM and satellite observation.

#### 743 **Acknowledgments**

744 This study is supported by the National Natural Science Foundation of China (No.  
745 41471343, 41425007 and 41101315) and the Chinese National Programs on Heavy  
746 Air Pollution Mechanisms and Enhanced Prevention Measures (Project No. 8 in the  
747 2nd Special Program).

748 **Author contributions.** LL designed this study. LL, YYY and WX conducted the data  
749 analysis. All co-authors contributed to the revision of the paper.

750 **Data availability.** OMI NO<sub>2</sub> datasets are available at  
751 <http://www.temis.nl/airpollution/no2.html>. IASI NH<sub>3</sub> datasets are available at  
752 <https://cds-espri.ipsl.upmc.fr/etherTypo/index.php?id=1700&L=1>. Surface NO<sub>2</sub>  
753 concentration during 2005-2007 obtained by Nowlan et al. (Nowlan et al., 2014) and  
754 longterm estimates (1996-2012) by Geddes et al. (Geddes et al., 2016) are available at  
755 [http://fizz.phys.dal.ca/~atmos/martin/?page\\_id=232](http://fizz.phys.dal.ca/~atmos/martin/?page_id=232). Total oxidized N<sub>r</sub> deposition  
756 simulated by GEOS-Chem constrained with GOME, SCIAMACHY, and GOME-2

757 NO<sub>2</sub> retrievals during 1996-2014 (Geddes and Martin, 2017) is available at  
758 [http://fizz.phys.dal.ca/~atmos/martin/?page\\_id=1520](http://fizz.phys.dal.ca/~atmos/martin/?page_id=1520). A database of atmospheric N<sub>r</sub>  
759 concentration and deposition from the nationwide monitoring network in China is  
760 available at <https://www.nature.com/articles/s41597-019-0061-2>. Measured N<sub>r</sub>  
761 concentration and deposition datasets in the United States are available on the website:  
762 <https://www.epa.gov/outdoor-air-quality-data>. Measured surface NO<sub>2</sub> and NH<sub>3</sub>  
763 concentration datasets in Europe are available at  
764 <https://www.nilu.no/projects/ccc/emepdata.html>. Global surface NO<sub>2</sub> and NH<sub>3</sub>  
765 concentration data used to calculate the longterm trends in **Fig. 13** and **Fig. 14** have  
766 been released on the website: <https://zenodo.org/record/3546517#.Xj6I4GgzY2w>.

767 **Competing interests.** The authors declare no competing financial interests.

## 768 **Reference**

769 Amos, H. M., Jacob, D. J., Holmes, C. D., Fisher, J. A., Wang, Q., Yantosca, R. M.,  
770 Corbitt, E. S., Galarneau, E., Rutter, A. P., and Gustin, M. S.: Gas-particle partitioning  
771 of atmospheric Hg(II) and its effect on global mercury deposition, *Atmos. Chem.*  
772 *Phys.*, 11, 29441-29477, 2012.

773 Beer, R., Shephard, M. W., Kulawik, S. S., Clough, S. A., Eldering, A., Bowman, K.  
774 W., Sander, S. P., Fisher, B. M., Payne, V. H., Luo, M., Osterman, G. B., and Worden,  
775 J. R.: First satellite observations of lower tropospheric ammonia and methanol,  
776 *Geophys. Res Lett.*, 35, 1-5, 10.1029/2008GL033642, 2008.

777 Bobbink, R., Hicks, K., Galloway, J., Spranger, T., Alkemade, R., Ashmore, M.,  
778 Bustamante, M., Cinderby, S., Davidson, E., Dentener, F., Emmett, B., Erisman, J.-W.,  
779 Fenn, M., Gilliam, F., Nordin, A., Pardo, L., and De Vries, W.: Global assessment of  
780 nitrogen deposition effects on terrestrial plant diversity: a synthesis, *Ecological*

781 Applications, 20, 30-59, doi:10.1890/08-1140.1, 2010.

782 Boersma, K. F., Eskes, H. J., Dirksen, R. J., van der A, R. J., Veefkind, J. P., Stammes,  
783 P., Huijnen, V., Kleipool, Q. L., Sneep, M., Claas, J., Leitão, J., Richter, A., Zhou, Y.,  
784 and Brunner, D.: An improved tropospheric NO<sub>2</sub> column retrieval algorithm for the  
785 Ozone Monitoring Instrument, Atmospheric Measurement Techniques, 4, 1905-1928,  
786 10.5194/amt-4-1905-2011, 2011.

787 Canfield, D. E., Glazer, A. N., and Falkowski, P. G.: The evolution and future of  
788 Earth's nitrogen cycle, Science, 330, 192-196, 2010.

789 Cao, G. L., Zhang, X. Y., and Gong, S. L.: Emission inventories of primary particles  
790 and pollutant gases for China, Science Bulletin, 56, 781-788, 2011.

791 Cheng, M., Jiang, H., Guo, Z., Zhang, X., and Lu, X.: Estimating NO<sub>2</sub> dry deposition  
792 using satellite data in eastern China, Int. J. Remote Sens., 34, 2548-2565, 2013.

793 Coheur, P.-F., Clarisse, L., Turquety, S., Hurtmans, D., and Clerbaux, C.: IASI  
794 measurements of reactive trace species in biomass burning plumes, Atmos. Chem.  
795 Phys., 9, 5655-5667, 2009.

796 Crippa, M., Guizzardi, D., Muntean, M., Schaaf, E., Dentener, F., van Aardenne, J. A.,  
797 Monni, S., Doering, U., Olivier, J. G. J., Pagliari, V., and Janssens-Maenhout, G.:  
798 Gridded emissions of air pollutants for the period 1970–2012 within EDGAR v4.3.2,  
799 Earth Syst. Sci. Data, 10, 1987-2013, 10.5194/essd-10-1987-2018, 2018.

800 Dammers, E., Palm, M., Van Damme, M., Vigouroux, C., Smale, D., Conway, S.,  
801 Toon, G. C., Jones, N., Nussbaumer, E., Warneke, T., Petri, C., Clarisse, L., Clerbaux,  
802 C., Hermans, C., Lutsch, E., Strong, K., Hannigan, J. W., Nakajima, H., Morino, I.,

803 Herrera, B., Stremme, W., Grutter, M., Schaap, M., Wichink Kruit, R. J., Notholt, J.,  
804 Coheur, P. F., and Erisman, J. W.: An evaluation of IASI-NH<sub>3</sub> with ground-based  
805 Fourier transform infrared spectroscopy measurements, *Atmos. Chem. Phys.*, 16,  
806 10351-10368, 10.5194/acp-16-10351-2016, 2016.

807 David, F., M, C., U, S., MA, S., JN, C., S, R., LJ, S., A, J., B, G., and JN, G.: The  
808 global nitrogen cycle in the twenty-first century, *Philosophical Transactions of the*  
809 *Royal Society of London*, 368, 20130164, 2013.

810 Emmons, L., Walters, S., Hess, P., Lamarque, J.-F., Pfister, G., Fillmore, D., Granier,  
811 C., Guenther, A., Kinnison, D., and Laepple, T.: Description and evaluation of the  
812 Model for Ozone and Related chemical Tracers, version 4 (MOZART-4),  
813 *Geoscientific Model Development*, 3, 43-67, 2010.

814 Erisman, J. W., Sutton, M. A., Galloway, J., Klimont, Z., and Winiwarter, W.: How a  
815 century of ammonia synthesis changed the world, *Nat. Geosci.*, 1, 636-639, 2008.

816 Farquhar, G. D., Firth, P. M., Wetselaar, R., and Weir, B.: On the Gaseous Exchange  
817 of Ammonia between Leaves and the Environment: Determination of the Ammonia  
818 Compensation Point, *Plant Physiology*, 66, 710-714, 10.1104/pp.66.4.710, 1980.

819 Galloway, J. N., Dentener, F. J., Capone, D. G., Boyer, E. W., Howarth, R. W.,  
820 Seitzinger, S. P., Asner, G. P., Cleveland, C., Green, P., and Holland, E.: Nitrogen  
821 cycles: past, present, and future, *Biogeochemistry*, 70, 153-226, 2004a.

822 Galloway, J. N., Dentener, F. J., Capone, D. G., Boyer, E. W., Howarth, R. W.,  
823 Seitzinger, S. P., Asner, G. P., Cleveland, C. C., Green, P. A., Holland, E. A., Karl, D.  
824 M., Michaels, A. F., Porter, J. H., Townsend, A. R., and Vöösmary, C. J.: Nitrogen

825 Cycles: Past, Present, and Future, *Biogeochemistry*, 70, 153-226,  
826 10.1007/s10533-004-0370-0, 2004b.

827 Galloway, J. N., Townsend, A. R., Erisman, J. W., Bekunda, M., Cai, Z., Freney, J. R.,  
828 Martinelli, L. A., Seitzinger, S. P., and Sutton, M. A.: Transformation of the nitrogen  
829 cycle: recent trends, questions, and potential solutions, *Science*, 320, 889-892, 2008.

830 Geddes, J. A., Martin, R. V., Boys, B. L., and van Donkelaar, A.: Long-term trends  
831 worldwide in ambient NO<sub>2</sub> concentrations inferred from satellite observations,  
832 *Environmental Health Perspectives*, 124, 281, 2016.

833 Geddes, J. A., and Martin, R. V.: Global deposition of total reactive nitrogen oxides  
834 from 1996 to 2014 constrained with satellite observations of NO<sub>2</sub> columns, *Atmos.*  
835 *Chem. Phys.*, 17, 10071-10091, 2017.

836 Graaf, S. C. v. d., Dammers, E., Schaap, M., and Erisman, J. W.: How are NH<sub>3</sub> dry  
837 deposition estimates affected by combining the LOTOS-EUROS model with  
838 IASI-NH<sub>3</sub> satellite observations?, *Atmos. Chem. Phys.*, 18, 13173-13196,  
839 <https://doi.org/10.5194/acp-2018-133>, 2018.

840 Grell, G. A., Peckham, S. E., Schmitz, R., McKeen, S. A., Frost, G., Skamarock, W.  
841 C., and Eder, B.: Fully coupled “online” chemistry within the WRF model, *Atmos.*  
842 *Environ.*, 39, 6957-6975, 2005.

843 Hoesly, R. M., Smith, S. J., Feng, L., Klimont, Z., Janssens-Maenhout, G., Pitkanen,  
844 T., Seibert, J. J., Vu, L., Andres, R. J., Bolt, R. M., Bond, T. C., Dawidowski, L.,  
845 Kholod, N., Kurokawa, J. I., Li, M., Liu, L., Lu, Z., Moura, M. C. P., O'Rourke, P. R.,  
846 and Zhang, Q.: Historical (1750–2014) anthropogenic emissions of reactive gases and

847 aerosols from the Community Emissions Data System (CEDS), *Geosci. Model Dev.*,  
848 11, 369-408, 10.5194/gmd-11-369-2018, 2018.

849 Janssens, I. A., Dieleman, W., Luysaert, S., Subke, J. A., Reichstein, M., Ceulemans,  
850 R., Ciais, P., Dolman, A. J., Grace, J., Matteucci, G., Papale, D., Piao, S. L., Schulze,  
851 E. D., Tang, J., and Law, B. E.: Reduction of forest soil respiration in response to  
852 nitrogen deposition, *Nat. Geosci.*, 3, 315, 10.1038/ngeo844  
853 <https://www.nature.com/articles/ngeo844#supplementary-information>, 2010.

854 Jia, Y., Yu, G., Gao, Y., He, N., Wang, Q., Jiao, C., and Zuo, Y.: Global inorganic  
855 nitrogen dry deposition inferred from ground-and space-based measurements,  
856 *Scientific reports*, 6, 1-11, 2016.

857 Kharol, S. K., Martin, R. V., Philip, S., Boys, B., Lamsal, L. N., Jerrett, M., Brauer,  
858 M., Crouse, D. L., McLinden, C., and Burnett, R. T.: Assessment of the magnitude and  
859 recent trends in satellite-derived ground-level nitrogen dioxide over North America,  
860 *Atmos. Environ.*, 118, 236-245, 2015.

861 Kharol, S. K., Shephard, M. W., McLinden, C. A., Zhang, L., Sioris, C. E., O'Brien, J.  
862 M., Vet, R., Cady-Pereira, K. E., Hare, E., Siemons, J., and Krotkov, N. A.: Dry  
863 Deposition of Reactive Nitrogen From Satellite Observations of Ammonia and  
864 Nitrogen Dioxide Over North America, *Geophys. Res Lett.*, 45, 1157-1166,  
865 10.1002/2017GL075832, 2018.

866 Kim, T. W., Lee, K., Duce, R., and Liss, P.: Impact of atmospheric nitrogen deposition  
867 on phytoplankton productivity in the South China Sea, *Geophys. Res Lett.*, 41, 3156–  
868 3162, 2014.

869 Kuik, F., Lauer, A., Churkina, G., Denier van der Gon, H. A. C., Fenner, D., Mar, K.  
870 A., and Butler, T. M.: Air quality modelling in the Berlin-Brandenburg region using  
871 WRF-Chem v3.7.1: sensitivity to resolution of model grid and input data,  
872 Geoscientific Model Development Discussions, 9, 4339-4363, 2016.

873 Lamarque, J. F., Kiehl, J., Brasseur, G., Butler, T., Cameron - Smith, P., Collins, W.,  
874 Collins, W., Granier, C., Hauglustaine, D., and Hess, P.: Assessing future nitrogen  
875 deposition and carbon cycle feedback using a multimodel approach: Analysis of  
876 nitrogen deposition, *Journal of Geophysical Research: Atmospheres* (1984–2012), 110,  
877 2005.

878 Lamsal, L. N., Martin, R. V., van Donkelaar, A., Steinbacher, M., Celarier, E. A.,  
879 Bucsela, E., Dunlea, E. J., and Pinto, J. P.: Ground-level nitrogen dioxide  
880 concentrations inferred from the satellite-borne Ozone Monitoring Instrument, *J.*  
881 *Geophys. Res-Atmos.*, 113, 1-15, 10.1029/2007JD009235, 2008.

882 Lamsal, L. N., Martin, R. V., Parrish, D. D., and Krotkov, N. A.: Scaling relationship  
883 for NO<sub>2</sub> pollution and urban population size: a satellite perspective, *Environ. Sci.*  
884 *Technol.*, 47, 7855-7861, 2013.

885 Larkin, A., Geddes, J. A., Martin, R. V., Xiao, Q., Liu, Y., Marshall, J. D., Brauer, M.,  
886 and Hystad, P.: Global Land Use Regression Model for Nitrogen Dioxide Air  
887 Pollution, *Environ. Sci. Technol.*, 51, 6957-6964, 2017.

888 Larssen, T., Duan, L., and Mulder, J.: Deposition and leaching of sulfur, nitrogen and  
889 calcium in four forested catchments in China: implications for acidification, *Environ.*  
890 *Sci. Technol.*, 45, 1192-1198, 2011.

891 Levine, S. Z., and Schwartz, S. E.: In-cloud and below-cloud scavenging of Nitric  
892 acid vapor, *Atmospheric Environment* (1967), 16, 1725-1734,  
893 [https://doi.org/10.1016/0004-6981\(82\)90266-9](https://doi.org/10.1016/0004-6981(82)90266-9), 1982.

894 Li, Y., Thompson, T. M., Damme, M. V., Chen, X., Benedict, K. B., Shao, Y., Day, D.,  
895 Boris, A., Sullivan, A. P., and Ham, J.: Temporal and Spatial Variability of Ammonia  
896 in Urban and Agricultural Regions of Northern Colorado, United States, *Atmos. Chem.*  
897 *Phys.*, 17, 1-50, 2017.

898 Liu, H., Jacob, D. J., Bey, I., and Yantosca, R. M.: Constraints from  $^{210}\text{Pb}$  and  $^7\text{Be}$  on  
899 wet deposition and transport in a global three-dimensional chemical tracer model  
900 driven by assimilated meteorological fields, *J. Geophys. Res-Atmos.*, 106,  
901 12109-12128, [10.1029/2000JD900839](https://doi.org/10.1029/2000JD900839), 2001.

902 Liu, L., Zhang, X., Xu, W., Liu, X., Lu, X., Chen, D., Zhang, X., Wang, S., and Zhang,  
903 W.: Estimation of monthly bulk nitrate deposition in China based on satellite  $\text{NO}_2$   
904 measurement by the Ozone Monitoring Instrument, *Remote Sens. Environ.*, 199,  
905 93-106, 2017a.

906 Liu, L., Zhang, X., Xu, W., Liu, X., Lu, X., Wang, S., Zhang, W., and Zhao, L.:  
907 Ground Ammonia Concentrations over China Derived from Satellite and Atmospheric  
908 Transport Modeling, *Remote Sens.*, 9, 467, 2017b.

909 Liu, L., Zhang, X., Zhang, Y., Xu, W., Liu, X., Zhang, X., Feng, J., Chen, X., Zhang,  
910 Y., Lu, X., Wang, S., Zhang, W., and Zhao, L.: Dry Particulate Nitrate Deposition in  
911 China, *Environ. Sci. Technol.*, 51, 5572-5581, [10.1021/acs.est.7b00898](https://doi.org/10.1021/acs.est.7b00898), 2017c.

912 Liu, L., Zhang, X., Wong, A. Y. H., Xu, W., Liu, X., Li, Y., Mi, H., Lu, X., Zhao, L.,



913 Wang, Z., and Wu, X.: Estimating global surface ammonia concentrations inferred  
914 from satellite retrievals, *Atmos. Chem. Phys.*, 19, 12051-12066,  
915 10.5194/acp-2019-184, 2019.

916 Liu, L., Zhang, X., Xu, W., Liu, X., Wei, J., Wang, Z., and Yang, Y.: Global estimates  
917 of dry ammonia deposition inferred from space-measurements, *Sci.Total Environ.*,  
918 730, 139189, <https://doi.org/10.1016/j.scitotenv.2020.139189>, 2020.

919 Liu, X., Duan, L., Mo, J., Du, E., Shen, J., Lu, X., Zhang, Y., Zhou, X., He, C., and  
920 Zhang, F.: Nitrogen deposition and its ecological impact in China: An overview,  
921 *Environ. Pollut.*, 159, 2251-2264, <http://dx.doi.org/10.1016/j.envpol.2010.08.002>,  
922 2011.

923 Liu, X., Xu, W., Duan, L., Du, E., Pan, Y., Lu, X., Zhang, L., Wu, Z., Wang, X.,  
924 Zhang, Y., Shen, J., Song, L., Feng, Z., Liu, X., Song, W., Tang, A., Zhang, Y., Zhang,  
925 X., and Collett, J. L.: Atmospheric Nitrogen Emission, Deposition, and Air Quality  
926 Impacts in China: an Overview, *Curr. Pollut. Rep.*, 3, 65-77,  
927 10.1007/s40726-017-0053-9, 2017d.

928 Lu, X., Jiang, H., Zhang, X., Liu, J., Zhang, Z., Jin, J., Wang, Y., Xu, J., and Cheng,  
929 M.: Estimated global nitrogen deposition using NO<sub>2</sub> column density, *Int. J. Remote*  
930 *Sens.*, 34, 8893-8906, 2013.

931 Mari, C., Jacob, D. J., and Bechtold, P.: Transport and scavenging of soluble gases in  
932 a deep convective cloud, *J. Geophys. Res-Atmos.*, 105, 22255-22268, 2000.

933 Nadelhoffer, K. J., Emmett, B. A., Gundersen, P., Kjønnaas, O. J., Koopmans, C. J.,  
934 Schleppei, P., Tietema, A., and Wright, R. F.: Nitrogen deposition makes a minor

935 contribution to carbon sequestration in temperate forests, *Nature*, 398, 145,  
936 10.1038/18205, 1999.

937 Nemitz, E., Flynn, M., Williams, P. I., Milford, C., Theobald, M. R., Blatter, A.,  
938 Gallagher, M. W., and Sutton, M. A.: A Relaxed Eddy Accumulation System for the  
939 Automated Measurement of Atmospheric Ammonia Fluxes, *Water, Air and Soil*  
940 *Pollution: Focus*, 1, 189-202, 10.1023/A:1013103122226, 2001.

941 Nicolas, G., and Galloway, J. N.: An Earth-system perspective of the global nitrogen  
942 cycle, *Nature*, 451, 293-296, 2008.

943 Nowlan, C., Martin, R., Philip, S., Lamsal, L., Krotkov, N., Marais, E., Wang, S., and  
944 Zhang, Q.: Global dry deposition of nitrogen dioxide and sulfur dioxide inferred from  
945 space-based measurements, *Global Biogeochem. Cy.*, 28, 1025-1043, 2014.

946 Paerl, H. W., Gardner, W. S., Mccarthy, M. J., Peierls, B. L., and Wilhelm, S. W.:  
947 Algal blooms: noteworthy nitrogen, *Science*, 346, 175, 2014.

948 Pan, Y., Wang, Y., Tang, G., and Wu, D.: Wet and dry deposition of atmospheric  
949 nitrogen at ten sites in Northern China, *Atmos. Chem. Phys.*, 12, 6515-6535, 2012.

950 Ronsmans, G., Langerock, B., Wespes, C., Hannigan, J. W., Hase, F., Kerzenmacher,  
951 T., Mahieu, E., Schneider, M., Smale, D., Hurtmans, D., De Mazière, M., Clerbaux, C.,  
952 and Coheur, P. F.: First characterization and validation of FORLI-HNO<sub>3</sub> vertical  
953 profiles retrieved from IASI/Metop, *Atmos. Meas. Tech.*, 9, 4783-4801,  
954 10.5194/amt-9-4783-2016, 2016.

955 Schrader, F., Brümmer, C., Flechard, C. R., Wichink Kruit, R. J., van Zanten, M. C.,  
956 Zöll, U., Hensen, A., and Erisman, J. W.: Non-stomatal exchange in ammonia dry

957 deposition models: comparison of two state-of-the-art approaches, *Atmos. Chem.*  
958 *Phys.*, 16, 13417-13430, 10.5194/acp-16-13417-2016, 2016.

959 Shen, J., Li, Y., Liu, X., Luo, X., Tang, H., Zhang, Y., and Wu, J.: Atmospheric dry  
960 and wet nitrogen deposition on three contrasting land use types of an agricultural  
961 catchment in subtropical central China, *Atmos. Environ.*, 67, 415-424,  
962 <http://dx.doi.org/10.1016/j.atmosenv.2012.10.068>, 2013.

963 Stevens, C. J., Dise, N. B., Mountford, J. O., and Gowing, D. J.: Impact of Nitrogen  
964 Deposition on the Species Richness of Grasslands, *Science*, 303, 1876-1879,  
965 10.1126/science.1094678, 2004.

966 Sutton, M. A., Tang, Y. S., Miners, B., and Fowler, D.: A New Diffusion Denuder  
967 System for Long-Term, Regional Monitoring of Atmospheric Ammonia and  
968 Ammonium, *Water Air & Soil Pollution Focus*, 1, 145-156, 2001.

969 Sutton, M. A., Bleeker, A., Howard, C. M., Bekunda, M., Grizzetti, B., Vries, W. D.,  
970 Grinsven, H. J. M. V., Abrol, Y. P., Adhya, T. K., and Billen, G.: Our Nutrient World:  
971 the challenge to produce more food and energy with less pollution, 2013.

972 Tan, J., Fu, J. S., Dentener, F., Sun, J., Emmons, L., Tilmes, S., Sudo, K., Flemming,  
973 J., Jonson, J. E., and Gravel, S.: Multi-model study of HTAP II on sulfur and nitrogen  
974 deposition, *Atmos. Chem. Phys.*, 18, 1-36, 2018.

975 Van Damme, M., Clarisse, L., Dammers, E., Liu, X., Nowak, J., Clerbaux, C.,  
976 Flechard, C., Galy-Lacaux, C., Xu, W., and Neuman, J.: Towards validation of  
977 ammonia (NH<sub>3</sub>) measurements from the IASI satellite, *Atmospheric Measurement*  
978 *Techniques*, 7, 12125-12172, 2014a.

979 Van Damme, M., Wichink Kruit, R., Schaap, M., Clarisse, L., Clerbaux, C., Coheur, P.  
980 F., Dammers, E., Dolman, A., and Erisman, J.: Evaluating 4 years of atmospheric  
981 ammonia (NH<sub>3</sub>) over Europe using IASI satellite observations and LOTOS-EUROS  
982 model results, *J. Geophys. Res-Atmos.*, 119, 9549-9566, 2014b.

983 Van der Graaf, S. C., Dammers, E., Schaap, M., and Erisman, J. W.: Technical note:  
984 How are NH<sub>3</sub> dry deposition estimates affected by combining the LOTOS-EUROS  
985 model with IASI-NH<sub>3</sub> satellite observations?, *Atmos. Chem. Phys.*, 18, 13173-13196,  
986 10.5194/acp-18-13173-2018, 2018.

987 Vet, R., Artz, R. S., Carou, S., Shaw, M., Ro, C.-U., Aas, W., Baker, A., Bowersox, V.  
988 C., Dentener, F., Galy-Lacaux, C., Hou, A., Pienaar, J. J., Gillett, R., Forti, M. C.,  
989 Gromov, S., Hara, H., Khodzher, T., Mahowald, N. M., Nickovic, S., Rao, P. S. P., and  
990 Reid, N. W.: A global assessment of precipitation chemistry and deposition of sulfur,  
991 nitrogen, sea salt, base cations, organic acids, acidity and pH, and phosphorus, *Atmos.*  
992 *Environ.*, 93, 3-100, <http://dx.doi.org/10.1016/j.atmosenv.2013.10.060>, 2014.

993 Vitousek, P. M., Aber, J. D., Howarth, R. W., Likens, G. E., Matson, P. A., Schindler,  
994 D. W., Schlesinger, W. H., and Tilman, D. G.: Human alteration of the global nitrogen  
995 cycle: sources and consequences, *Ecol. Appl.*, 7, 737-750, 1997.

996 Wei, J., Huang, W., Li, Z., Xue, W., Peng, Y., Sun, L., and Cribb, M.: Estimating  
997 1-km-resolution PM<sub>2.5</sub> concentrations across China using the space-time random  
998 forest approach, *Remote Sens. Environ.*, 231, 111221,  
999 <https://doi.org/10.1016/j.rse.2019.111221>, 2019.

1000 Wesely, M., and Hicks, B.: Some factors that affect the deposition rates of sulfur

1001 dioxide and similar gases on vegetation, *Journal of the Air Pollution Control*  
1002 *Association*, 27, 1110-1116, 1977.

1003 Whitburn, S., Van Damme, M., Clarisse, L., Bauduin, S., Heald, C. L., Hadji-Lazaro,  
1004 J., Hurtmans, D., Zondlo, M. A., Clerbaux, C., and Coheur, P. F.: A flexible and robust  
1005 neural network IASI-NH<sub>3</sub> retrieval algorithm, *J. Geophys. Res-Atmos.*, 121,  
1006 6581-6599, 10.1002/2016JD024828, 2016.

1007 Williams, J. E., Boersma, K. F., Le Sager, P., and Verstraeten, W. W.: The  
1008 high-resolution version of TM5-MP for optimized satellite retrievals: description and  
1009 validation, *Geosci. Model Dev.*, 10, 721-750, 10.5194/gmd-10-721-2017, 2017.

1010 Wong, D. C., Pleim, J., Mathur, R., Binkowski, F., Otte, T., Gilliam, R., Pouliot, G.,  
1011 Xiu, A., Young, J. O., and Kang, D.: WRF-CMAQ two-way coupled system with  
1012 aerosol feedback: software development and preliminary results, *Geosci. Model Dev.*,  
1013 5, 299-312, 10.5194/gmd-5-299-2012, 2012.

1014 Xu, W., Luo, X. S., Pan, Y. P., Zhang, L., Tang, A. H., Shen, J. L., Zhang, Y., Li, K. H.,  
1015 Wu, Q. H., Yang, D. W., Zhang, Y. Y., Xue, J., Li, W. Q., Li, Q. Q., Tang, L., Lv, S. H.,  
1016 Liang, T., Tong, Y. A., Liu, P., Zhang, Q., Xiong, Z. Q., Shi, X. J., Wu, L. H., Shi, W.  
1017 Q., Tian, K., Zhong, X. H., Shi, K., Tang, Q. Y., Zhang, L. J., Huang, J. L., He, C. E.,  
1018 Kuang, F. H., Zhu, B., Liu, H., Jin, X., Xin, Y. J., SHi, X. K., Du, E. Z., Dore, A. J.,  
1019 Tang, S., Collett Jr, J. L., Goulding, K., Sun, Y. X., Ren, J., Zhang, F. S., and Liu, X. J.:  
1020 Quantifying atmospheric nitrogen deposition through a nationwide monitoring  
1021 network across China, *Atmos. Chem. Phys.*, 15, 12345-12360, 2015.

1022 Yu, G., Jia, Y., He, N., Zhu, J., Chen, Z., Wang, Q., Piao, S., Liu, X., He, H., Guo, X.,

1023 Wen, Z., Li, P., Ding, G., and Goulding, K.: Stabilization of atmospheric nitrogen  
1024 deposition in China over the past decade, *Nat. Geosci.*, 12, 424-429,  
1025 10.1038/s41561-019-0352-4, 2019.

1026 Zhang, L., Wright, L. P., and Asman, W. A. H.: Bi-directional air-surface exchange of  
1027 atmospheric ammonia: A review of measurements and a development of a big-leaf  
1028 model for applications in regional-scale air-quality models, *J. Geophys. Res-Atmos.*,  
1029 115, 898-907, 2010.

1030 Zhang, L., Jacob, D. J., Knipping, E. M., Kumar, N., Munger, J. W., Carouge, C., Van  
1031 Donkelaar, A., Wang, Y., and Chen, D.: Nitrogen deposition to the United States:  
1032 distribution, sources, and processes, *Atmos. Chem. Phys.*, 12 4539-4554, 2012.

1033 Zhang, Q., Streets, D. G., Carmichael, G. R., He, K., Huo, H., Kannari, A., Klimont,  
1034 Z., Park, I., Reddy, S., and Fu, J.: Asian emissions in 2006 for the NASA INTEX-B  
1035 mission, *Atmos. Chem. Phys.*, 9, 5131-5153, 2009.

1036 Zhang, X. Y., Lu, X. H., Liu, L., Chen, D. M., Zhang, X. M., Liu, X. J., and Zhang, Y.:  
1037 Dry deposition of NO<sub>2</sub> over China inferred from OMI columnar NO<sub>2</sub> and atmospheric  
1038 chemistry transport model, *Atmos. Environ.*, 169, 2017.

1039 Zhang, X. Y., Chuai, X. W., Liu, L., Zhang, W. T., Lu, X. H., Zhao, L. M., and Chen,  
1040 D. M.: Decadal Trends in Wet Sulfur Deposition in China Estimated From OMI SO<sub>2</sub>  
1041 Columns, *J. Geophys. Res-Atmos.*, 123, 10796-10811, 10.1029/2018JD028770, 2018.

1042 Zhao, X., Chen, L., and Zhang, H.: Nitrate and ammonia contaminations in drinking  
1043 water and the affecting factors in Hailun, northeast China, *Journal of Environmental*  
1044 *Health*, 75, 28, 2013.

1045 Zhao, Y., Zhang, L., Chen, Y., Liu, X., Xu, W., Pan, Y., and Duan, L.: Atmospheric  
1046 nitrogen deposition to China: A model analysis on nitrogen budget and critical load  
1047 exceedance, *Atmos. Environ.*, 153, 32-40,  
1048 <http://dx.doi.org/10.1016/j.atmosenv.2017.01.018>, 2017.  
1049